Palaeogeography, Palaeoclimatology, Palaeoecology 560 (2020) 110017

Contents lists available at ScienceDirect

Palaeogeography, Palaeoclimatology, Palaeoecology

journal homepage: www.elsevier.com/locate/palaeo

Invited Research Article

Cyclostratigraphy and astrochronology: Case studies from China

Chunju Huang[a,b], James G. Ogg[a,c,d,*], David B. Kemp[a]

[a] State Key Laboratory of Biogeology and Environmental Geology, School of Earth Sciences, China University of Geosciences, Wuhan 430074, China
[b] Hubei Key Laboratory of Critical Zone Evolution, School of Earth Sciences, China University of Geosciences, Wuhan 430074, China
[c] State Key Laboratory of Oil and Gas Reservoir Geology and Exploitation, Chengdu University of Technology, Chengdu 610059, China
[d] Department of Earth, Atmospheric and Planetary Sciences, Purdue University, 550 Stadium Mall Drive, West Lafayette, IN 47907-2051, USA

ARTICLE INFO

Keywords:
Milankovitch cycles
Orbital cycles
Climate change
Astronomical time scale
Sequences

ABSTRACT

A high-precision geologic time scale is the essential key for understanding the Earth's evolutionary history and geologic processes. Astronomical tuning of orbitally forced stratigraphic records to construct high-resolution Astronomical Time Scales (ATS) has led to a progressive refinement of the geologic time scale over the past two decades. In turn, these studies provide new insights regarding the durations and rates of major Earth events, evolutionary processes, and climate changes, all of which provide a scientific basis for contextualizing and predicting future global change trends. South China hosts some of the best-exposed and well-dated Neoproterozoic through Mesozoic stratigraphic sections in the world; many of which are suitable for cyclostratigraphy and calibrating the geologic time scale. In North China, several Cenozoic oil-bearing basins have deep boreholes with continuous sampling and/or well logging that enable derivation of astronomically tuned time scales for an improved understanding of basin evolution and hydrocarbon generation. This Special Issue focuses on case studies of astrochronology and applied cyclostratigraphy research using reference sections within China. In this introductory overview, we: (1) summarize all existing astrochronology studies of the Neoproterozoic through Cenozoic sections within China that have been used to enhance the international geologic time scale, (2) examine briefly the astronomically forced paleoclimate information recorded in various depositional systems and the modern techniques employed to analyze the periodicity of these signals encoded within the sedimentary record, and (3) summarize the 20 contributions to this Special Issue of *Palaeogeography, Palaeoclimatology, Palaeoecology* on 'Cyclostratigraphy and Astrochronology: Case studies from China'.

1. Introduction

Astronomically induced variations in Earth's precession and obliquity modulate seasonal insolation and drive climate changes in the Earth system (Hinnov, 2018). The Earth's seasons are caused by the obliquity (tilt) of its rotation axis relative to the Sun. The Earth's orbit around the Sun is slightly elliptical (= eccentricity); therefore, the relative average summer temperature in a hemisphere depends upon whether its summer occurs during the Earth's furthest distance from the Sun (aphelion; which is the current situation for the Northern Hemisphere) or during its closest approach (perihelion). The precession of the Earth's rotation axis relative to its orbit causes a ca. 20-kyr cycle in the relative warmth of a hemisphere's summer (and coldness of its winter) as it oscillates between aphelion to perihelion conditions. The eccentricity of the Earth's orbit is influenced by the gravitational attraction of other planets, and changes from nearly circular (the current situation with a relatively low importance of precession-induced climatic change) to a more elliptical orbit that causes greater seasonal contrasts. Eccentricity varies with a ca. 100-kyr oscillation that is further modulated by a 405-kyr cycle. Superimposed on the precession-eccentricity signal are ca. 40-kyr periodic variations of the obliquity of the Earth's axis; and these are especially important in influencing seasonal contrasts at higher latitudes.

Together, these variations in the relative differences in summer heat versus winter cooling are called "Milankovitch cycles" after Milutin Milanković, the Serbian mathematician who did the initial detailed numerical analysis of the effects on solar insolation at different latitudes (Milankovitch, 1930, 1941). These long-term orbital-induced climate cycles are also manifested as changes in many different geographic and sedimentary processes, including average seasonal rainfall and fluvial runoff, ice cap size, global sea level, types and amount of vegetation, rates and styles of continental weathering, the position and intensity of wind belts, monsoon patterns, coastal currents, and the supply and recycling of nutrients within both marine and lacustrine waters. In turn,

* Corresponding author.
E-mail addresses: huangcj@cug.edu.cn (C. Huang), jogg@purdue.edu (J.G. Ogg), davidkemp@cug.edu.cn (D.B. Kemp).

https://doi.org/10.1016/j.palaeo.2020.110017

Available online 11 September 2020
0031-0182/

sediment influxes into all depositional systems, from continental lacustrine sediments to deep-sea deposits, undergo shifts in the relative ratios of coarse-to-fine siliciclastics and of terrigenous to biogenic components, and in the relative importance of storm and flood events. Consequently, the periodic climatic changes attributable to orbital forcing are readily encoded in stratigraphic successions, and cyclostratigraphers can measure chemical and physical proxies (e.g., elemental concentrations, grain size, magnetic susceptibility, etc.) that track these cycles in order to identify astronomical signals. One challenge to this endeavor is that the recording of Milankovitch cycles in the sedimentary record is superimposed upon a wide spectrum of non-periodic variability, and sedimentary systems are prone to shifts in accumulation rates and sediment composition induced by non-Milankovitch factors such as regional tectonics, temporally irregular shifting of fluvial-delta depocenters, and other trends.

The first published application of this cyclostratigraphic "clock in the rock" concept was by G.K. Gilbert (1895), who used it to estimate elapsed time in Upper Cretaceous deposits in North America. The discipline became more widely established after the seminal work by Hays et al. (1976), which demonstrated pervasive astronomial control on climate changes across the past ~0.5 million years. Since then, the astronomical theory has been widely studied and applied. During the past two decades in particular, astronomical calibration of stratigraphic successions has been successfully used to constrain the Cenozoic and Mesozoic geologic time scales, aided by the development of numerical solutions of Earth's orbit across the past ~50 million years by Jacques Laskar et al. (1993, 2004, 2011).

China hosts superb Neoproterozoic and Mesozoic stratigraphic sections in marine facies, as well as lacustrine deposits encompassing large portions of the Permian through Neogene, and thick accumulations of wind-blown loess spanning the Quaternary. Cyclostratigraphic analyses of proxy data from outcrops and boreholes within China have been important for calibrating the geologic time scale, understanding basin evolution and oil-forming mechanisms, and for unraveling the impacts of past glacial-interglacial climate oscillations. This special issue of *Palaeogeography, Palaeoclimatology, Palaeoecology* brings together 20 papers that highlight the importance of Chinese sections for cyclostratigraphy and time scales. The studies cover a wide range of stratigraphic records in marine and terrestrial deposits within China, and incorporate aspects of biostratigraphy, lithostratigraphy, chemostratigraphy, magnetostratigraphy, and radioisotopic dating.

In this introductory review paper, we present two summaries of cyclostratigraphy studies in China. We first summarize all the cyclostratigraphy studies of sections within China that present astronomical time scales that enable high-resolution enhancement of the geologic time scale (Ediacaran through Quaternary). Six of these are also part of this Special Issue (Fang et al., 2020; Lu et al., 2019; Ma et al., 2019; Ma et al., 2020a; Sui et al., 2019; Zhong et al., 2019b). The second group are those that apply cyclostratigraphy and astronomically tuned depositional rates to better understand basin development and Earth system evolution during portions of the Neoproterozoic through Cenozoic (Chu et al., 2020; Du et al., 2020; Gong et al., 2019; Li et al., 2020; Liu et al., 2020; Peng et al., 2020; Xu et al., 2019; Xu et al., 2020; Yao and Hinnov, 2019; Zhang et al., 2019a, 2019b; Zhang et al., 2020; Zhang 2019; Zhao et al., 2019).

2. Geologic settings of the sedimentary records of China

The sedimentary history of regions within China were particularly conducive to recording climate cycles in relatively stable depositional settings. The South China Craton was a part of the Gondwana continental margin during the Cryogenian through Silurian; then, as a separate island mini-plate from the Devonian through middle Triassic, it accumulated a thick carbonate platform adjacent to eroding "oldlands". Consequently, South China hosts some of the best-exposed and well-dated Neoproterozoic, Paleozoic and Mesozoic stratigraphic sections in the world. The exceptional nature of these fossiliferous and well-preserved marine deposits is why South China hosts nearly a dozen GSSPs (Global Stratigraphic Section and Point) of stratigraphic boundaries for the Paleozoic and early Mesozoic geologic stages. Equally, these reference sections have provided cyclostratigraphic records for calibrating the durations of biozones and other events of the international geologic time scale.

Basins within other blocks that now comprise China contained large lakes at tropical to temperate latitudes. In addition to accumulating organic-rich deposits that became important oil and gas source rocks, these lacustrine deposits were particularly conducive to recording climate-induced fluctuations in the relative influx of clay and organic carbon. Cyclostratigraphic studies of these lacustrine deposits have often utilized records from deep boreholes and range from the Permian through Neogene. In particular, North China has several Cenozoic oil-bearing basins with deep boreholes that have been continuously sampled and/or well-logged for cyclostratigraphy studies.

During the Quaternary and continuing to the present, windblown dust from the arid interior regions of central Asia accumulated as thick loess deposits in the middle watershed of the Yellow River and elsewhere. During more humid intervals, such as major interglacial episodes, reddish soil horizons developed on these loess plains; and the resulting alternation of arid-climate loess and humid-climate soil has enabled astronomical calibration of Eurasia's glacial episodes.

3. Astronomical Time Scale studies using reference sections in China

As of July 2020, there have been over 30 cyclostratigraphy studies of marine, lacustrine or loess deposits that have direct application to enhancing the age model for the geologic time scale (Table 1, Fig. 1). Studies of these are part of this Special Issue of *Palaeogeography, Palaeoclimatology, Palaeoecology,* including contributions on the Ediacaran (Sui et al., 2019), Cambrian (Fang et al., 2020) and Ordovician-Silurian (Lu et al., 2019; Zhong et al., 2019b; Ma et al., 2020b; Ma et al., 2019). Only the Cenozoic and the Jurassic of China, for which there is a lack of extensive uplifted exposures of fossiliferous marine strata, have not yielded cyclostratigraphic studies that are directly applicable to improving the geologic time scale. However, the entire Cenozoic time scale and much of the Jurassic has been cycle-tuned based on ocean drilling boreholes, uplifted oceanic sediments in the Mediterranean region, and borehole and outcrop studies in Britain and other regions.

As expected from its geologic history, nearly all of the Ediacaran, Paleozoic and Triassic cyclostratigraphy studies have been undertaken on the South China Craton (Fig. 1). The exceptions are Ordovician studies in the Tarim Basin, which included the auxiliary GSSP for the Middle/Late Ordovician boundary (Sandbian GSSP), and in Hebei Province of North China. North China has cyclostratigraphy studies of Cretaceous terrestrial basins that helped to calibrate the evolution of feathered dinosaurs (Wu et al., 2013b) and of magnetic polarity chrons. The thick loess deposits in Shaanxi Province allowed calibration of the major Quaternary climate oscillations and the development of desert regions of eastern Asia (e.g., Ding et al., 2002).

Nearly all studies on pre-Cenozoic Chinese reference sections recognized the dominant 405-kyr long-eccentricity modulation of the precession cycle within marine or lacustrine deposits. In contrast to the theoretical lengthening of the periods for Earth's precession and obliquity through geologic time due to the influence of its Moon, the 405-kyr long-eccentricity cycle has had a stable period for at least the past half-billion years (e.g., Hinnov, 2018). This 405-kyr signal in the sedimentary record enables an "astronomical tuning" of a meter-scale record yielding a "floating" time scale. The resulting durations of geologic stages and of corresponding biozones, geochemical excursions, and magnetic polarity zones derived by these studies generally have a precision of ~0.1 Myr (i.e., one quarter of a long-eccentricity cycle). In the case of Songliao Basin borehole in northeastern China, radio-

Table 1

Summary of astrochronology studies on Chinese reference sections that are used to enhance the geologic time scale. Abbreviations: (1) Proxies – MS = magnetic susceptibility, GR = natural gamma-ray radiation, ARM = anhysteretic remanent magnetization, XRF = X-ray fluorescence; (2) Method – MTM = multi-taper method, Evol. spectra = evolutive spectra; (3) Cycles – E = long-eccentricity, e = short-eccentricity, O = obliquity, P = precession; (4) Other – U-Pb = uranium-lead dating (Ding et al., 1994, Lu et al., 1999, Heslop et al., 2000; Deng et al., 2019a; Deng et al., 2019b; Sun et al., 2006; Wu et al., 2014; Wang et al., 2016; Deng et al., 2013; Wang et al., 2016; Wu et al., 2009; Xi et al., 2019; Wu et al., 2013a; He et al., 2012; Wu et al., 2013b; Zhu et al., 2007a,b; Liu et al., 2017a,b; Huang, 2019; Li et al., 2017; Tong et al., 2019; Zhang et al., 2015; Lehrmann et al., 2015; Li et al., 2016a,b; Li et al., 2007; Wu et al., 2012; Zhao et al., 2005; Wu et al., 2013c; Shen et al., 2011; Mundil et al., 2004; Yuan et al., 2019; Xue et al., 2015; Shen et al., 2019; Xue et al., 2015; Fang et al., 2017; Mei et al., 1994; Fang et al., 2015; Fang et al., 2012; Ueno et al., 2013; Wang et al., 2019a,b; Zhang et al., 2019a, 2019b, 2019c, 2019d, 2019e, 2019f; Ueno et al. (2013); Wu et al., 2018; Qi et al., 2014; Ross and Ross, 1988; Li et al., 1997; Rygel et al., 2008; Ueno et al., 2013; Bai, 1995b; Qie et al., 2019; Gong et al., 2001; Gong et al., 2005; Huang et al., 2016; Rong et al., 2019; Chen et al., 2018; Chen et al., 2011; Ma et al., 2019a; Wang et al., 2018; Ma et al., 2016; Ma et al., 2019b; Ma et al., 2019c; Peng et al., 2009; Chen et al., 2006; Zhu et al., 2019a,b; McFadden et al., 2008; Condon et al., 2005; Zhou et al., 2019;Bai et al., 1982; Bai et al., 1994; Li et al., 2009; Zhong et al., 2018; Bai, 1995a; Chen et al., 2015; Fang et al., 2019, Gong et al., 2017, Hu and Qi, 2017; Sui et al., 2018, Wang et al., 2009, Zhong et al., 2018).

(*continued on next page*)

Table 1 (*continued*)

Table 1 -- Summary of astrochronology studies on Chinese reference sections used to enhance the geologic time scale

#	Author (* =Corresp. if different), publication	Geologic System (Stage)	What was calibrated	Result	Location	Main studied facies; thickness, depos. environ.; Age control	(1) Proxies; (2) Method	Main cycle for tuning (implied span of record); Other recorded cycles	Raw data provided?	(1) Associated paleontology or age control; (2) Other studies; (3) Reviews; (4) Other information
1	Ding, Z.L., et al., 2002, Paleocean., 17: 1033.	Quaternary	Loess and paleosol cycles (arid/humid)	Loess-paleosol alternations mainly correlate to marine delta-Oxy18 cycles for past 1.8 Myr.	Shaanxi-Gansu border, Southern and middle Loess plateau (Baoji (34.4°N, 107.1°E, Lingtai (35.1°N, 107.6°E), Jingchuan (35.3°N, 107.4°E) and Pingliang (35.6°N, 106.7°E)	Silt, paleosol; ca. 160 m average; wind-blown dust; Magnetostratigraphy	(1) Grain size; (2) Assumed in-phase relation to global ice volume for tuning	Obliquity and precession filters (33 main paleosols (Baoji section); 2.6 Myr)	Upon request to Ding, Z.L.	(1) Sun, Y., et al., 2006, Quat. Sci. Rev., 25: 33-48. (2) Ding et al., 1994, Quat. Sci. Rev., 13: 39-70; Lu, H., et al., 1999, Palaeo-3, 154: 237-246; Heslop et al., 2000, EPSL, 184: 125-139. (3) Deng, C.J., et al., 2019, Sci. China Earth Sci., 62: 324-348 -- Other scales "have been established by tuning paleoclimatic proxy records ... taking into account the lock-in depth offsets of geomagnetic polarity reversals in loess and/or the lags between solar insolation forcing and the monsoon climate response." "Constrained by those high-precision astronomical timescales, it is reasonable to conclude that for the CLP, loesspaleosol sequence units L0 and S0 correspond to the Holocene; units L1 and S1, to the Salawusuan Stage of the Upper Pleistocene; units from L2 to the upper part of L8, to the Zhoukoudianian Stage of the Middle Pleistocene; units from the middle-lower part of L8 to L33, to the Nihewanian Stage of the Lower Pleistocene; and units S33 and L34, to the Mazegouan Stage of the Upper Pliocene."
		Neogene -- no cyclostratigraphic studies in China applicable for enhancing geologic time scale								(3) Deng, T., et al., 2019, Sci. China Earth Sci., 62: 310-323..
		Paleogene -- no cyclostratigraphic studies in China applicable for enhancing geologic time scale								(3) Wang, Y.Q., 2019, Sci. China Earth Sci., 62: 287-309.
2	Wu, H.C., et al., 2014, EPSL, 407: 82-95.	Cretaceous (upper Santonian to lower Danian)	Magnetostratigraphy; spore-pollen, charophye and ostracod zones	Durations C30n-C31n (3.0 Myr), C31r (2.2 Myr), C32n (2.2 Myr), C32r (0.9 Myr), C33n-C33r (9.0 Myr). Base of Campanian (base of polarity chron C33r) revised to be 83.07 ±0.15 Ma (in companion article by Wang et al., 2016), then refined as 82.875 Ma (Wu et al., PNAS, in press).	Jilin Prov., Songliao Basin SK1 north (ca. 45.3°N, 125.0°E). Upper Cretaceous in "SK1" is composite of two boreholes ca. 77 km apart in the south-central part of the basin	Lacustrine claystone-siltstone; 1542 m; deep lake to shallow lake; U-Pb dates	(1) Thorium component of GR; (2) MTM, Evol. spectra, band-pass filters, tuning	405-kyr E (~30 m) for tuning (37 cycles; ca. 15 Myr plus ca. 4 Myr hiatus); also e, O, P, Modulations of 1.36 and 2.05 Myr	Suppl. text table (12550 Th-depth pts)	(1) Deng, C.L. et al., 2013, Palaeo-3, 385: 44-54; Wang, T.T., et al., 2016, EPS,L 446:37-44. (2) Wu, H.C., et al., 2009, EPSL 278: 308-323. (3) Xi, D.P. et al., 2019, Sci. China Earth Sci., 62: 256-286.
3	Wu, H.C., et al., 2013a, Palaeo-3, 383: 55-70.	Cretaceous (lower Turonian to lower Campanian)	Magnetostratigraphy; ostracod zones	Base of Campanian (base of polarity Chron C33r) is 83.63 Ma (but see 2014 and 2020 revisions above). Brief R-subzones in C34n in lower Santonian at ca. 84.85, 85.0 and 85.5 Ma.	Jilin Prov., Songliao Basin SK1 south (ca. 44.5°N, 125.2°E). SK1 Upper Cretaceous is composite of two boreholes ca. 77 km apart in the south-central part of the basin	Lacustrine claystone-siltstone; 950 m; deep lake; U-Pb dates	(1) MS, GR; (2) MTM, Evol. spectra, band-pass filters, tuning	405-kyr E (~35 m) for tuning (21 cycles; 8.9 Myr); also e, O, P. Modulations of 1.2 and 2.34 Myr	**No**	(1) He et al., 2012, Geochem, Geophys, Geosys, 13, Q02002.
4	Wu, H.C., et al., 2013b, Palaeo-3, 385: 221-228.	Cretaceous (lower)	Jehol vertebrate beds; Magnetostrat	Feathered dinosaur interval spans only ca. 0.15 Myr. Entire normal-polarity unit is ca. 0.86 Myr, which could be M3n.	W Liaoning Prov. (Beipiao; Sihetun outcrop; 41.59°N, 120.79°E)	Lacustrine claystone with volcanic ash; 11.2 m; U-Pb dates (ca. 126-124 Ma)	(1) MS, ARM; (2) MTM, Evol. spectra, band-pass filters, tuning	100 kyr e (~2 m) for tuning (6.7 cycles; 0.7 Myr); also O, P	**No**	(1) Zhu, R.X., et al., 2007, Cret. Res., 28: 171-176; (2) Liu, Z., et al., 2017, Palaeo-3, 481: 44-56.
		Jurassic -- no cyclostratigraphic studies in China applicable for enhancing geologic time scale								(3) Huang, D.,et al., 2019, Sci. China Earth Sci., 62: 223-255.
5	Li, M.S., et al., 2017 (Huang, C.J.*), EPSL 474: 207-223.	Triassic (upper Norian-Rhaetian)	Magnetostrat	Verifies cycle-durations of latest 6.5 Myr of Triassic polarity scale from Newark Group. Age of the earliest dinosaur footprints in China is 2.5 Myr before end of Triassic (middle Rhaetian; ca. 204 Ma).	Sichuan Prov. (roadcuts of Xujiahe 32.49°N, 105.85°E;, Zilanba 32.42°N, 105.65°E; Qilixia 31.20°N, 107.74°E; and Tanba 29.93°N, 106.38°E)	Siltstone and sandstone; ca. 600 m; lacustrine-fluvial; Magnetostrat (same paper)	(1) MS, GR; (2) MTM, Evol. spectra, band-pass filters, tuning	405-kyr E (~55 m) for tuning (16.5 cycles; 6.7 Myr); also e	Suppl. Excel table (ca. 3600 GR, 1200 MS pts)	(3) Tong, J.N., et al 2019, Sci. China Earth Sci., 62: 189-222. (4) A follow-up 13Corg study verified a negative excursion within same magneto-cycle zone (one 405-kyr cycle from base of Newark E20r) as projected from Italy that has been suggested as a potential Rhaetian GSSP marker level (Li, M.S., et al., 2017).
6	Zhang, Y., et al., 2015 (Ogg, J.G.*), Palaeo-3, 146: 135-166.	Triassic (lower Carnian)	Magnetostrat of Early Carnian (Julian substage)	Early Carnian is dominated by a 1.3 Myr reversed-polarity zone.	Guizhou Prov. (Wayao outcrop, 25.89°N, 105.42°E; and Zhenfeng, Laishike outcrop, 25.57°N, 105.49°E)	Limestone, with clay-rich uppermost Julian; ca. 150 m merged composite; carbonate shelf-slope; Conodonts	(1) GR; (2) MTM, Evol. spectra, band-pass filters, tuning	405-kyr E (~34 m) for tuning (6 cycles; 2.4 Myr); also e, P	Suppl. Excel table (ca. 550 GR pts)	
7	Li, M.S., Huang, C.J.*, et al., 2018a, EPSL, 482: 591-606.	Triassic (Anisian)	International geologic stage (Frasnian); Conodont and magnetic-polarity zones	Anisian Stage 5.3 Myr; durations of substages, of 6 condont zones (or pairs of zones) and of 9 pairs of magnetic-polarity zones.	Guizhou Prov. (Luodian, Guandao outcrops, 25.61°N, 106.62°E)	Limestone; 330 m (265 m after removing breccias); slope; Conodonts	(1) GR, MS; (2) MTM, Evol. spectra, band-pass filters, tuning	405-kyr E (~3 m) for tuning (15 cycles; 6.2 Myr); also e, O, P	Suppl. Excel table (1070 GR and 2060 MS pts)	(1) Lehrmann et al., 2015, J. Asian Earth Sci., 108: 117-135. (4) Cyclostratigraphy analysis required removing major breccia layers. Merged with Early Triassic cyclostrat (Li, M.S., et al., 2016) for 26 E-cycle scaling of base-Triassic through earliest Ladinian stages, substages, delta-13C, and magnetic polarity.
8	Li, M.S., et al., 2016a (Huang, C.J.*), EPSL, 441: 10-25.	uppermost Permian through Triassic (Induan, Olenekian)	International geologic stages (Induan, Olenekian) and substages; Conodont and magnetic-polarity zones	Induan Stage 2.0 Myr (Griesbachian substage 1.4 ±0.1 Myr, Dienerian 0.6 ±0.1 Myr), Olenekian Stage 3.3 Myr (Smithian 1.7 ±0.1 Myr, Spathian 1.4 ±0.1 Myr); durations of China regional conodont zones and estimated for 10 pairs of magnetic-polarity zones.	Anhui Prov. (Chaohu quarries with candidate GSSP of Olenekian, 31.63°N, 117.83°E), Hubei Prov. (Daxiakou roadcut, 31.11°N, 110.80°E), Zhejiang Prov. (Meishan GSSP of Triassic, 31.08°N, 119.71°E), Guizhou Prov. (Luodian, Guandao outcrop, 25.61°N, 106.62°E)	Induan is mainly claystone and marl; Olenekian is mainly limestone with much higher accumulation rate; merged composite is ca. 300 m; Conodonts, Magnetostrat to Germanic Basin	(1) GR, (2) MTM, Evol. spectra, band-pass filters, tuning	405-kyr E (ca. 10 m average) for tuning (15 cycles of which 3 are in Permian; 6.5 Myr); also e, O, P	Suppl. Excel table (total of 5000 GR pts for 3 sections)	(1) numerous paleontology and delta-C13 studies on these 4 major reference sections. (2) Li, S., et al., 2007, Palaeo-3, 252: 188-199.
9	Wu, H.C., et al., 2012, Gond. Res., 22: 748-759.	Triassic (Induan)	International geologic stage (Induan), substages. Conodont zones	Induan Stage 1.2 Myr (Griesbachian substage 0.5 Myr, Dienerian 0.7 Myr); durations of 6 China regional conodont zones.	Hubei Prov. (Daxiakou roadcut, 31.11°N, 110.80°E)	Mainly claystone and marl; Conodonts	(1) MS, ARM; (2) MTM, band-pass filters, tuning	405-kyr E (ca. 12 m) for tuning (5 cycles; 2 Myr); also e, P	**No**	(1) Zhao, L.S., et al., 2005, Albertiana, 33: 113-114; Li, H., et al.,, 2009, Earth Sci. - J. China Univ. Geosci., 34: 733-742.
10	Wu, H.C., et al., 2013c, Nat. Comm., 4: 2452	Permian (Lopingian)	International geologic epoch (Lopingian epoch); Conodont zones; end Permian extinction	Lopingian Epoch 7.79 Myr; durations of 11 conodont zones.	Zhejiang Prov. (GSSP of Triassic at Meishan, 31.083°N, 119.706°E), Sichuan Prov. (Shangsi section, 32.333°N, 105.467°E)	Wuchiapingian through middle Changhsingian stages are mainly siliceous micrite limestone with cherts; Uppermost Changhsingian to lowest Induan is mainly calcareous shales with thin-bedded limestones; carbonate platform/slope then intraplatform; Conodonts, U-Pb dates	(1) MS, ARM; (2) U–Pb age-calibration; MTM, Evol. spectra, band-pass filters, tuning relative to Perm-Tri GSSP as 252.10 Ma	405-kyr E (~8 m) for tuning (5 cycles; 2 Myr) in Meishan; 405-kyr E (~15 m for lower part and ~2 m for upper part) for tuning (21 cycles; 8.4 Myr) in Shangsi; also e, O, P; Modulations of 3.45, 1.93, 1.26, 1.02 Myr (ecc) and 3.11, 0.57 Myr (obl).	**No**	(1) Shen, S.Z., et al., 2011, Science, 334: 1367-1372; Mundil et al., 2004, Science, 305: 1760-1763. (3) Yuan, D.X., et al., 2019, Sci. China Earth Sci., 62: 190-209.

(*continued on next page*)

Table 1 (*continued*)

#	Author (* =Corresp. if different), publication	Geologic System (Stage)	What was calibrated	Result	Location	Main studied facies; thickness, depos. environ.; Age control	(1) Proxies; (2) Method	Main cycle for tuning (implied span of record); Other recorded cycles	Raw data provided?	(1) Associated paleontology or age control; (2) Other studies; (3) Reviews; (4) Other information
11	Xue, W.Q., et al., 2015, Chinese J. Geophys., 58: 611-627.	Permian (Capitanian)	International geologic stage (Capitanian); Conodont zones	Capitanian Stage spans 3.85 ±0.28 Myr. Capitanian conodont zones *Jinogondolella postserrata* (0.15 Myr), *J. shannoni* (0.06), *J. altudaensis* (2.30), *J. prexuanhanensis* (0.77), *J. xuanhanensis* (0.46), *J. granti* (0.08), and *Clarkina postbitteri hongshuiensis* (0.03 Myr).	Guangxi Prov. (Laibin, Tieqiao, Wuchiapingian GSSP; 23.6953°N, 109.3211°E)	Chert and limestone; slope-basin; Conodonts (that study)	(1) MS; (2) MTM, Fourier analysis, tuning	405-kyr E (~12 m) for tuning (15 cycles; 4 Myr); also e, O, P.	**?**	(3) Shen, S.Z., et al., 2019, Sci. China Earth Sci., 62: 154-188.
12	Fang, Q, Wu, H.C.*, et al., 2017, Palaeo-3, 474, 130-139.	Permian (Wordian, Capitanian)	International geologic stage (Capitanian); Conodont zones	Capitanian Stage spans 2.65 Myr, but with ca. 0.8 Myr no-data below. Capitanian conodont zones *Jinogondolella postserrata* (0.5 Myr, but with ca. 0.8 Myr no-data below), *J. altudaensis* (0.56 Myr), *J. prexuanhanensis* (0.82), and *J. xuanhanensis* (0.75). Wordian zone *J. asserata(* >2.4 Myr).	Sichuan Prov. (Dukou section; 31.70°N, 108.30°E)	Limestone; 49 m; carbonate slope; Conodonts	(1) MS, ARM; (2) MTM, Evol. spectra, band-pass filters, tuning	405-kyr E (~3 m) for tuning (15 cycles; 6 Myr); also e, O, P. Modulations of 1 Myr	**No**	(1) Mei, S.L., et al., 1994, Acta Palaeont. Sinica, 33: 1-23. (4) "The estimated astronomical durations of the Jinogondolella postserrata ..., J. altudaensis ..., J. prexuanhanensis ...,, and J. xuanhanensis ... zones are 490 kyr, 560 kyr, 820 kyr, and 750 kyr, respectively. However, the durations of these same conodont zones derived from the basinal facies successions in the Tieqiao section, South China have been estimated as 150 kyr, 2300 kyr, 770 kyr, and 460 kyr, respectively (Xue et al., 2015). The significant variation in conodont zone durations between different sections may be due to diachrony of the biozones or the different sedimentary settings." (quote from Fang et al., 2017)
13	Fang, Q. Wu, H.C.*, et al., 2015, Palaeo-3, 440: 848-859.	Permian (Roadian, Wordian, Capitanian)	International geologic stages (Roadian, Wordian); Conodont zones	Roadian (3.7 ±0.4 Myr) and Wordian (2.9 ±0.4 Myr) durations.	N. Sichuan Prov. (Shangsi section, 32.33°N, 105.47°E)	Limestone; 201 m; slope; Conodonts	(1) ARM; (2) MTM, Evol. spectra, band-pass filters, tuning	405-kyr E (~7 to 15 m) for tuning (24 cycles; 4 Myr); also e, O, P. Modulations of 2.0 Myr (ecc.) and 1.0 Myr (obl.)	**No**	(1) Fang, Q., et al., 2012, J. Strat., 36: 692-699.
14	Ueno, K., et al., 2013, Geol. Soc. Lond. Spec. Publ., 376: 235-267.	Carboniferous (Moscovian through Gzhelian) and Early Permian	International Stages; Fusulinid zones	Some major lowstand exposure surfaces correlate with major cyclothems in Midcontinent USA and Moscow basin; but not all of those cyclothems are resolved.	Guizhou Prov. (Zongdi section, ca. 30 km SE of Ziyun on country road connecting to Luodian, 25.589°N, 106.352°E)	Limestone; 360 m; shallow-marine; Fusulinids	(1) Lowstand exposure surfaces; (2) Seq. Strat. analysis	405-kyr E (indirectly) (21 depositional sequences in Upper Pennsylvanian; but the 5 recognized in Asselian may have "skipped beats")	Detailed stratigraphy log diagrams	(2) Zhang, B., et al., 2019, J. Geol. Soc., 176: 588-608. (3) Wang, X.D., et al., 2019, Sci. China Earth Sci., 62: 135-153. (4) "Ueno et al. (2013) studied high-resolution Pennsylvanian cyclothems in the Zongdi section, Ziyun, Guizhou, South China, using fusulinid biostratigraphy. A total of 21 depositional sequences (DS), separated by subaerial exposure surfaces, were recognized in Moscovian (8 DS), Kasimovian (5 DS), and Gzhelian (8 DS) strata. The duration of each sequence is about 400–450 ka, consistent with an eccentricity driver."
15	Wu, H.C. et al., 2018, Geology, 47: 83-86.	Carboniferous (Serpukhovian through Gzelian)	International Stages (5); regional Conodont zones (25)	Serpukhovian 7.6 Myr; Bashkirian 8.1 Myr; Moscovian 8.5 Myr; Kasimovian 2.87 Myr; Gzhelian 4.83 Myr durations.	S Guizhou Prov. (Naqing roadcut; 25.25°N 106.49°E); Candidate GSSPs for Serpukhovian, Moscovian, Kasimovian and Gzhelian.	Limestone; 250 m; carbonate slope; Conodonts	(1) MS; (2) MTM, Evol. spectra, band-pass filters, tuning	405-kyr E (~3 m) for tuning (83.7 cycles; 33.9 Myr); also e, O, P. Modulations of 1.2, 1.6, 2.4 Myr	Suppl. Excel table (5000 pts)	(1) Qi, Y.P., et al., 2014, Geol. Mag., 151: 254-268; Hu, K.Y., and Qi, Y.P., 2017, Strat., 14: 197-215. (2) "Development of depositional sequences and high-frequency cycles during the Carboniferous was closely related to the waxing and waning of Gondwanan glaciation (Ross and Ross, 1988; Li et al., 1997; Rygel et al., 2008; Ueno et al., 2013)." from (3) Wang, X.D., et al., 2019, Sci. China Earth Sci., 62: 135-153.
16	Fang, Q., Wu, H.C*., et al., 2018, J. Asian Earth Sci., 156: 302-315.	Carboniferous (Serpukhovian through Moscovian)	International Stages (Serpukhovian); regional Conodont zones	Serpukhovian 7.68 ±0.15 Myr duration.	S Guizhou Prov. (Luokun section; 25.31°N 106.57°E)	Limestone; 170 m; carbonate slope; Conodonts	(1) MS; (2) MTM, Evol. spectra, band-pass filters, tuning	405-kyr E (~3.5 m) for tuning (26 cycles; 10.5 Myr); also e, O, P. Modulations of 1.2 Myr (obl.), and 2.4 with lesser 1.2 and 1.6 Myr (ecc.)	**No**	(4) Base of Moscovian is a hiatus => no cyclostratigraphy duration for the underlying Bashkirian
17	Ma, K.Y., et al., 2020 (Gong, Y.M.*), Glob. Plan. Change, 193: 103267	Devonian (Famennian)	International geologic stage (Famennian); Conodont zones	Famennian 14.4 ±0.28 Myr duration; scaling of 20 component conodont zones and 12 bio-environmental events and/or sequences.	Guangxi Prov. (Lali section, 50 km W of Yizhou City; 24.45°N, 108.29°E)	Limestone; 180 m studied; inter-platform trough to slope; Conodonts	(1) XRF-Ca; (2) MTM, Evol. spectra, band-pass filters adjusted to changing sed-accum-rate, tuning	405-kyr E (8 to 3.5 m) for tuning (35.5 cycles; 14.4 Myr); also e, O, P	**No**	(1) Zhang, X.S., et al., 2019, Palaeo-3, 531: 109219. (4) Suppl. has sediment accum. rate; conodont ranges; etc.. but no raw data.
18	Bai, S.L., 1995b, Internat. Geol. Rev., 37: 1109-1114	Devonian (Middle through Upper)	International geologic stages (Emsian through Famennian); Conodont zones	u. Emsian 4.4 Myr, Eifelian 3.2 Myr, Givetian 5.3 Myr, Frasnian 5.0 Myr, Famennian 9.4 Myr *(monograph publications not available at this time)*	Guangxi and Hunan Prov. (several sections; Lat-Long not given) *(monograph publications not available at this time)*	Limestone; Conodonts	(1) Geochemistry (Al, Ni/La, etc.)	100-kyr "e" ?	**?**	(1) Bai, S.L., monograph of 1982; (2) Bai, S.L., monographs of 1994, 1995a. (3) Qie, W.K. et al., 2019, Sci. China Earth Sci., 62: 112-134 -- "Bai et al. ... indicated that the 100 kyr period in chemical element abundances and ratios ... [is a] response to the orbital perturbations of eccentricity." (4) Monographs with the details were not available during compilation of this review due to Covid-19 library closures.
19	Gong, Y.M., et al., 2001, Palaeo-3, 168:237-248.	Devonian (Frasnian-Famennian)	Conodont zones	upper *rhenana* Zone 0.6 Myr, *linguiformis* Zone 0.8 Myr, *triangularis* Zone 0.9 Myr (with 3 equal subzones).	Guizhou (Yangd and Longmem outcrops) and Guangxi (Du'an and Liujing outcrops)	Clayey limestone; slope to basin; Conodonts	(1) Bedding hierarcy; (2) Counting Bundles, bundle sets, superbundles; correlating among sections	Superbundle as E (ca. 3 m); also e, O, P	Detailed stratigraphic diagrams	
20	Gong, Y.M., et al., 2005, Sci. China D Earth Sci., 48: 32-41.	Devonian (Frasnian-Famennian)	International geologic stage (Frasnian); Conodont zones	Frasnian Stage 4.3 Myr. Durations of 12 condont zones: *falsiovalis* 0.4 Myr, transitans 0.4 Myr, *punctata* 0.4 Myr, Lower and upper *hassi* 0.3 and 0.4 Myr, *jamieae* 0.2 Myr, Lower and upper *rhenana* 0.8 and 0.2 Myr, *linguiformis* 0.8 Myr, Lower-middle-upper *triangularis* 0.3 Myr each.	Guangxi *(source publications not available at this time)*	carbonate-basin and slope facies (source publications not available at this time); Conodonts	(1) Bedding hierarcy; (2) Counting Bundles, bundle sets, superbundles; correlating among sections	Superbundle as E; also e, O, P	**?**	(4) Frasnian Stage of 4.3 Myr is less than half of its ca. 9.5 Myr duration in GTS 2012
21	Huang, C.J., et al., 2016, GSA Ann. Mtg., 127-2.	Ordovician-Silurian (Katian-Aeronian)	International geologic stage (Hirnantian); Graptolite zones	Hirnantian Stage 1.46 Myr; Rhuddanian graptolite zones *A. ascensus* (1.1 Myr) and *P. acuminatus* (1.3 Myr).	Sichuan and W Hubei prov. (Shuange, Qijiang, Wangjiawan sections; and 4 borehole logs)	Calcareous claystone; deep water; Graptolites	(1) XRF; (2) MTM, Evol. spectra, band-pass filters, tuning	405-kyr E for tuning (ca. 35 cycles; 14 Myr)	**No**	(3) Rong, J.Y., et al., 2019, Sci. China Earth Sci., 62: 89-111. (4) For this study; there was only an advance abstract with the indicated information. Not yet published as full paper.

(*continued on next page*)

Table 1 (*continued*)

#	Author (* =Corresp. if different), publication	Geologic System (Stage)	What was calibrated	Result	Location	Main studied facies; thickness, depos. environ.; Age control	(1) Proxies; (2) Method	Main cycle for tuning (implied span of record); Other recorded cycles	Raw data provided?	(1) Associated paleontology or age control; (2) Other studies; (3) Reviews; (4) Other information
22	Lu, Y.B., Huang, C.J.*, et al., 2019, Palaeo-3, 526: 96-109.	Ordovician (upper Katian-Hirnantian)	International geologic stage (Hirnantian); Graptolite zones	Hirnantian Stage 1.74 ±0.4 Myr; Late Katian graptolite zones *D. complanatus* (0.6 Myr), *D. complexus* (0.8 Myr), *P. pacificus* (1.8 Myr).	W Hubei Prov. (Yichang, borehole EHD1; 30.10°N, 110.14°E)	Black siliceous claystone with carbonate layers and ash beds; 9.1 m; low-oxygen depression; Graptolites (projected)	(1) XRF (Fe signal) at 1-cm intervals; (2) MTM, Evol. spectra, band-pass filters, tuning	405-kyr E (0.75 m) for tuning (12.25 cycles; 5.0 Myr); also e, O, P. obliquity-modulations of 1.2 Myr.	**No**	(1) Chen, X., et al, 2018, Sci. China Earth Sci., 61: 1195-1203. (3) Zhang, Y.D., et al., 2019, Sci. China Earth Sci., 62: 61-88.
23	Zhong, Y.Y., Wu, H.C*., et al., 2019, Palaeo-3, 540: 109520.	Ordovician (upper Katian-Hirnantian)	International geologic stage (Hirnantian); Graptolite zones	Hirnantian Stage 1.26 Myr; Late Katian graptolite zones *D. complexus* (1.3 Myr), *P. pacificus* (1.8 Myr).	NE Yunnan Prov. (Wanhe roadcut; 27.76°N, 103.48°E)	Calcareous claystone; 48.5 m; deep-water; Graptolites (projected)	(1) MS; (2) MTM, Evol. spectra, band-pass filters, tuning	405-kyr E (3 m) for tuning (18 cycles; 7.37 Myr); also e, O, P. Modulations of 1.3 Myr (obl.),and 2.4 and 1.4 Myr (ecc.)	Suppl. Excel table (2677 pts)	(1) Projected from Tang, P., et al., 2017, J. Strat., 41: 119-133.
24	Zhong, Y.Y., et al., 2019 (Fan, J.X.*), Acta Geo. Sinica, 93: 177-180.	Ordovician (upper Sandbian-lower Katian)	Regional conodont and equivalent graptolite zones	Graptolite zones *O. calcaratus* through *D. gravis* span 5.98 Myr. Pagoda Lms Fm spans 2.4 Myr.	W Hubei Prov. (Yichang, Huanghuachang borehole YH-1 near Hirnantian GSSP; 30.88°N, 111.40°E)	Limestone; 28 m; Yangtze Platform; Conodonts	(1) MS, GR, Oxy-18; (2) MTM, Evol. spectra, band-pass filters, tuning	405-kyr E (2 m) for tuning (14.5 cycles; 5.98 Myr); also e, O, P	**No**	(1) Chen, X., et al., 2011, Earth Env. Sci. Trans., R. Soc. Edinburgh, 101: 111-134; (4) This 5.98 Myr interval spanned 8.25 Myr in GTS2016, which implies that overlying upper Katian graptolite zones in Wufeng Fm must have much longer durations than as scaled in GTS2016. This is supported by unpublished U-Pb ID-TIMS ages (Fan, J.X., oral commun. to J.Ogg, 2019)
25	Ma, X.Y., Deng, S.H.*, et al., 2020, Palaeo-3, in review.	Ordovician (Sandbian-lower Katian)	Delta13C excursion (GICE)	Sandbian > 6.4 Myr. Latest Sandbian-early Katian Positive 13-C excursion ("GICE") spans ca. 4 Myr. Pagoda Lms Fm spans 5.5 to 6 Myr.	NE Sichuan Prov. (Qiaoting, Bazhong, 32.46°N, 106.89°E), SE Sichuan (Xikou, Huaying, 30.16°N, 106.69°E); Chongqing (Sanquanzhen Nanchuan, 29.14°N, 107.19°E), N Guizhou Prov. (Liangcun, Xishui 28.46°N, 106.35°E)	Limestone; Pagoda Limestone, 32 m; Yangtze Platform; Conodonts	(1) MS; (2) MTM, Evol. spectra, band-pass filters, tuning	405-kyr E (ca. 2 m) for tuning (33 cycles lower Sandbian through top of e. Katian Pagoda Lms; 13.6 Myr); also e, O, P	**?**	(1) Ma, X.Y., et al., 2019a, J. Strat., 43: 1-10; Wang, Z.H., et al., 2018, Acta Micro. Sinica, 35: 13-29; and other publ.; (2) Ma, K.Y., et al., 2016, Earth Sci. Front., 23: 268-286; Ma, X.Y., et al., 2019b, Acta. Petr. Sinica, 40: 577-586; Ma, X.Y. et al., 2019c, Earth Sci. Front., 26 :281-291. (4) GICE excursion is more complete in the southern sections on the Yangtze Platform.
26	Fang, Q., Wu, H.C.*, et al., 2019, Glob. Plan. Change, 173: 96-108.	Ordovician (Darriwilian, lower Sandbian)	Regional graptolite and equivalent conodont zones	Darriwilian Graptolite zones *Pterograptus elegans* (1.04 Myr), *Didymograptus murchisoni* (2.12 Myr) and *Jiangxigraptus vagus* (0.54 Myr).	Xinjiang Prov. (N. Tarim Basin, Kalpin: Dawangou stream cut - Sandbian Aux. GSSP 40.72°N, 79.54°E; and Yangikan stream cut 40.43°N, 79.17°E)	Claystone (Dawangou), Siliceous limestone (Yangikan);12 and 70 m; basin and slope; Graptolites, Conodonts	(1) MS, GR; (2) MTM, Evol. spectra, band-pass filters, tuning	405-kyr E (ca. 1 m Dawangou, ca. 3 m Yangikan) for tuning (12 and 17 cycles; 4.9 and 6.8 Myr); also e, O, P. Modulation of obliquity (1.2 Myr) and eccentricity (2.4 Myr).	**No**	(1) Zhen, Y.Y., et al., Records Aust. Mus., 63: 203-266; Chen, X., et al., 2015, monograph; and other publ. (4) The cyclostratigraphy has extended intervals of dominance by obliquity forcing.
27	Zhong, Y.Y., Wu, H.C.*, et al., 2018, Palaeo-3, 505: 86-99.	Ordovician (Darriwilian, Dapingian)	International geologic stages (Darriwilian, Dapingian); Graptolite zones	Darriwilian 8.38 ±0.4 Myr; Dapingian 1.97 ±0.7 Myr.	Zhejiang Prov. (Huangnitang GSSP for Darriwilian, and adjacent Changjin borehole CJ-3; 28.87°N, 118.49°E)	Black claystone, limestone; 48 m; deep-water slope; Graptolites	(1) MS; (2) MTM, Evol. spectra, band-pass filters, tuning	405-kyr E (ca. 2 m) for tuning (29 cycles; 12.4 Myr); also e, O, P. Modulations of 1.2 and 2.4 Myr.	Suppl. Excel table (MS 3913 horizons)	(1) Chen, X., et al., 2006, Palaeoworld, 15: 150-170.
28	Ma, K.Y, et al., 2019 (Gong, Y.M.*), Palaeo-3, 528: 272-287.	Ordovician (Floian)	International geologic stage; Conodont zones	Floian Stage 7.08 ±0.4 Myr; Conodont zones *S. bilobatus* 1.0 Myr, *S. extensus* 5.1 Myr, *O. communis* 0.2 Myr, *O. evae* 0.8 Myr, and *B. triangularis* 0.2 Myr.	W Hubei Prov. (Yichang, Huanghuachang GSSP for Dapingian 30.8605°N, 110.37°E) and Hebei Prov. (Liangjiashan section; 40.10°N, 119.59°E)	Limestones, 41 m and 112 m, both shallow shelf; Conodonts	(1) XRF-Ca and Fe/Ca; (2) MTM, Evol. spectra, band-pass filters, tuning	405-kyr E (ca. 5 m Huanghuachang; ca. 7 m Liangjiashan) for tuning (totals of 7.5 and 18.5 cycles; 3.0 and 7.0 Myr); also e, O, p. Modulations of 1.0 and 1.9 Myr.	Suppl. Excel table (1033 and 514 Ca-value horizons for the 2 sections)	(1) Liangjiashan section -- conodont study is part of the cyclostrat paper. Huanghauchang GSSP -- Wang, X.F., et al., 2009, *Episodes*, **32**: 96–113. (4) Cyclostratigraphy analysis required removing distortions by storm beds.
29	Fang, J.C., Wu, H.C.*, et al., 2020, Palaeo-3, 540: 109530.	Cambrian (Drumian-Guzhangian)	Trilobite zones	Late Drumian trilobites zones *G. nathorsti* 0.52 Myr, *L. armata* 0.15 Myr; base-*Guzhangian L. laevigata* >0.7 Myr.	Hunan Prov. (Guzhang, Luoyixi (formerly Wangcun) roadcut = Guzhangian GSSP; 28.72°N, 109.97°E)	Clayey limestones, 87 m, mid-depth slope; Trilobites	(1) MS and 13-C; (2) MTM, Evol. spectra, band-pass filters, tuning	405-kyr E (ca. 25 m) for tuning (3.5 cycles; 1.4 Myr); also e, O, P	Suppl. Excel table (MS 4340 pts, Delta13C)	(1) Peng, S.C., et al., 2009, Episodes, 23: 41-55. (3) Zhu, M.Y. et al., 2019, Sci. China Earth Sci, 62: 25-60.
30	Sui, Y., Huang, C.J.*, et al., 2019, Palaeo-3, 532: 109273.	Ediacaran	Delta13C excursions (upper Dushantou Fm)	Shuram (EN3) excursion spans ca. 20 Myr. Onset relative to U-Pb date (551.1 ±0.7 Ma) at top of Doushantou Fm is ca. 571.1 ±0.8 Ma. Span of entire Doushantou Fm projected as 84 Myr.	W Hubei Prov. (5 km east of Three Gorges Dam, Jiulongwan roadcut; 30.80°N, 111.06°E)	Cherty dolomite and limestone, then black shale; 85 m; mid-depth shelf; 13C excursions; U-Pb dates near base and top of this section	(1) XRF-Fe; (2) MTM, Evol. spectra, band-pass filters, tuning	405-kyr E (ca. 1.5 m) for tuning (73 cycles; 29.7 Myr); also e, O, P. Modulations of 2.2 (ecc..)	**No**	(1) McFadden et al., 2008, PNAS, 105: 3197-3203; Condon et al., 2005, Science, 308: 95-98. (3) Zhou et al., 2019, Sci. China Earth Sci, 62: 7-24. (4) The analysis was done in 4 intervals due sediment-accumulation rate changes
31	Gong, Z., et al, 2017, Precamb. Res., 289: 62-74.	Ediacaran	Delta13C excursions (upper Dushantou Fm)	Shuram (EN3) excursion spans 9.1 ±1.0 Myr based on projected sediment accumulation rate. Onset relative to U-Pb date (551.1 ±0.7 Ma) at top of Doushantou Fm is ca. 560 Ma.	E Yunnan Prov. (Dongdahe roadcut; 24.70°N, 102.95°E)	Clayey limestone, then black shale; 45 m; shallow-water basin; 13C exursions	(1) MS, ARM; (2) MTM, Evol. spectra, band-pass filters	405-kyr E (ca. 4.3 m; 11 cycles; ca. 4.4 Myr); also e, O, P. Modulations of 2.4 (ecc..)	**No**	(1) Zhu, M., et al., 2007, Palaeo-3, 254: 7-61.
32	Sui, Y., Huang, C.J.*, et al., 2018, Sci. Bull., 63: 1485-1494.	Ediacaran	Delta13C excursions (lower Dushantou Fm)	Cap carbonate span projected as 1.6 Myr; First large acritarchs and multi-cellular animal embryos at 3.8 Myr after end of cap carbonate.	W Hubei Prov. (5 km east of Three Gorges Dam, Jiulongwan roadcut; 30.80°N, 111.06°E)	Cap-carbonate, then organic-rich claystone and dolomite; 22 m; mid-depth shelf, lower Doushantuo Formation, 22 m; 13C excursions; U-Pb dates near base	(1) XRF-Fe/Ti and Ca; (2) MTM, Evol. spectra, band-pass filters, tuning	405-kyr E (ca. 0.9 m) for tuning (27 cycles; 11.2 Myr); also e, O, P. Modulations of 1.2 (obl.)	**No**	(1) McFadden et al., 2008, PNAS, 105: 3197-3203; Condon et al., 2005, Science, 308: 95-98.
33	Bao, X.J., Zhang, S.H.*, et al., 2018, EPSL, 483: 52-63.	Cryogenian	Cryogenian interglacial	Duration of non-glacial Datangpo Fm is ca. 9.8 Myr. Nantuo (Marinoan) glaciation began at ca. 650 Ma relative to ca. 660 Ma date for end of Sturtian glaciation.	NE Guizhou Prov. (Songtao, borehole ZK1909; ca. 27.5°N 108°E?)	Clayey siltstone; 292 m; deep-water basin; U-Pb and Re-Os dates on termination of Sturtian on various continents	(1) MS; (2) MTM, Evol. spectra, band-pass filters, tuning	405-kyr E (ca. 14 m) for tuning (21 E cycles plus 10 e cycles; 9.8 Myr); also e, O, P	Suppl. PDF table (MS 28,765 pts)	

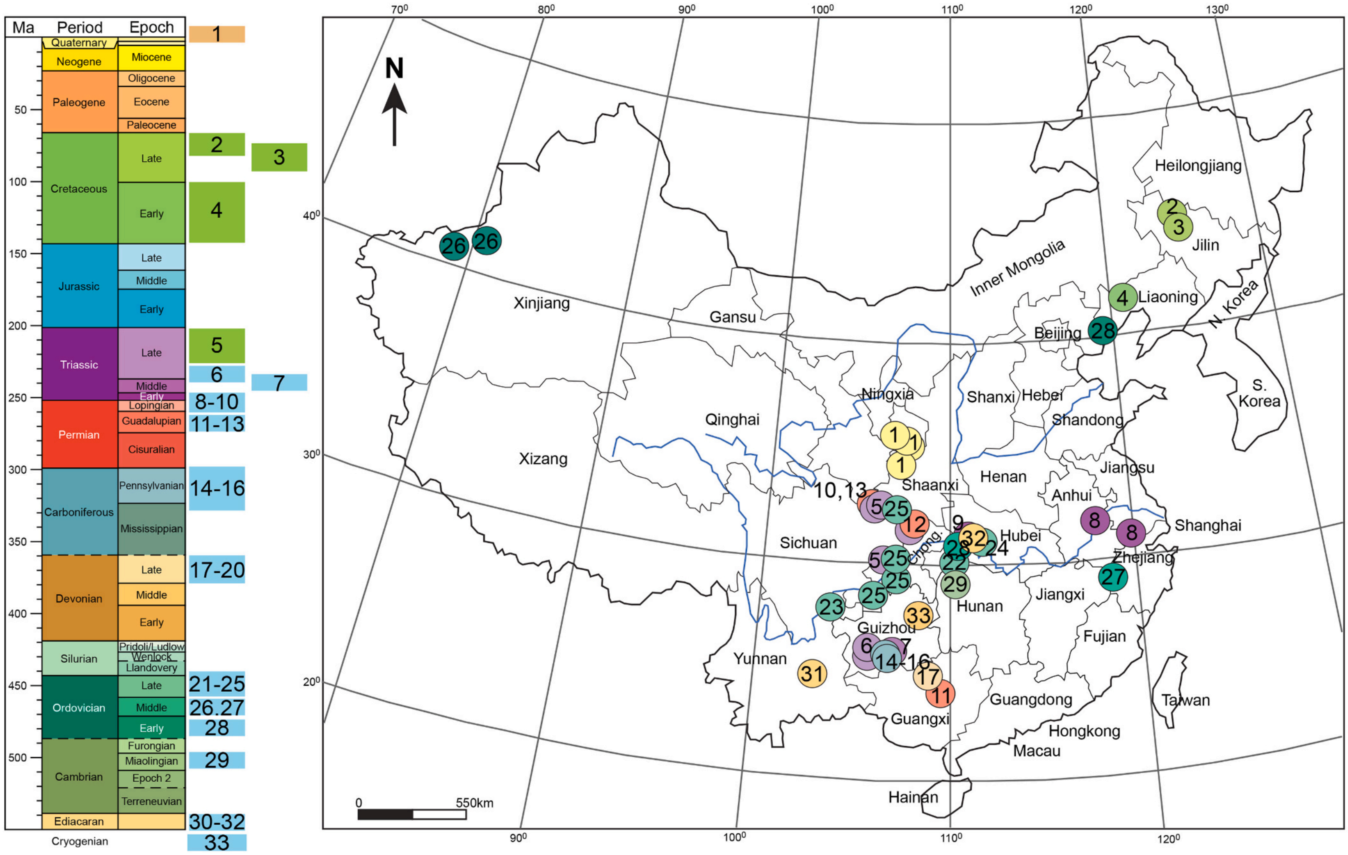

Fig. 1. Locations of cyclostratigraphy studies in China that are relevant to enhanced calibration of the geologic time scale. The color of each location dot is the same as the color of the geologic epoch. Coloring of the bars for the span of each study (next to the geologic time scale) indicates the general depositional setting (blue = marine, green = lacustrine, tan = other terrestrial). For details on each study, see the corresponding number in Table 1. (For interpretation of the references to color in this figure legend, the reader is referred to the web version of this article.)

isotopic dating has enabled the 405-kyr cycles within the Upper Cretaceous record to be anchored in absolute time by tying these to the corresponding cycles in the numerical solution of astronomical forcing (Laskar et al., 2011). This assigns an age of 82.9 Ma to the base of magnetic polarity Chron C33r, which is the candidate marker for the base of the Campanian Stage (Wu et al., 2020). Several of these cycle-scaled durations of stages and of other geologic episodes have been incorporated into the period-level syntheses of the integrated stratigraphy and timescale of China (right-hand column in Table 1) and into Neoproterozoic and Phanerozoic time scales (e.g., Ogg et al., 2016; and chapters within Gradstein et al., 2020).

4. Applications of cyclostratigraphy within China

The 20 cyclostratigraphy studies in this Special Issue (Table 2) span the Ediacaran through Pleistocene (Table 2). Of these, 6 are directly applicable to enhancing the geologic time scale, and therefore were also included in Table 1. The locations range from the Tibetan Plateau near the Himalayas to offshore Guangdong in the South China Sea (Fig. 2).

The majority of the 12 Mesozoic and Cenozoic studies in this Special Issue applied cyclostratigraphy to deposits in terrestrial basins, especially lacustrine and fluvial-delta sequences. Scientific questions include: establishing the relative timing of seismic horizons and the duration of oil- and gas-generating organic-rich source rocks (Du et al., 2020; Zhao et al., 2019; Xu et al., 2019; Peng et al., 2020; Liu et al., 2020; Chu et al., 2020; Zhang et al., 2019b), determining how glacial-interglacial oscillations influenced the influx of coarser-grained siliciclastics (Zhang et al., 2019a; Zhang et al., 2019a), and constraining the depositional history of deltas (Xu et al., 2020; Zhang et al., 2020). The biostratigraphic constraints in many of these deposits are limited to poorly age-calibrated terrestrial faunal and floral remains. As such, some of the floating astronomically tuned time scales are anchored using the "traditional" ages based on assigning certain seismic or other horizons to geologic stage boundaries. However, with the aid of the constraints on durations and relative timing of events from cyclostratigraphy, the widespread non-marine Mesozoic-Cenozoic facies of China have the potential to be tied to contemporaneous marine rocks elsewhere (and vice versa), emphasizing the utility of cyclostratigraphy for building timescales to correlate and understand climate evolution in terrestrial environments. In the future, it may be possible to improve those age models through recognition of longer-period astronomical cycles (so-called "grand cycles").

The eight Ediacaran and Paleozoic cyclostratigraphy studies in this Special Issue are on marine successions composed of carbonate, shale or chert. Scientific questions range from durations of graptolite, conodont and radiolarian zones (Yao and Hinnov, 2019; Lu et al., 2019; Zhong et al., 2019a; Ma et al., 2019; Fang et al., 2020) to the durations of carbon-isotope excursions (Ordovician GICE by Ma et al., 2020b; Ediacaran Shuram CIE by Gong et al., 2019, and Sui et al., 2019). The two studies on the Shuram CIE yielded quite different durations, estimated at ca. 9 Myr by Gong et al. (2019) versus ca. 20 Myr by Sui et al. (2019) (note: the shorter estimate was based on extrapolating a sedimentation rate from only a portion of the entire CIE).

Table 2

Summary of cyclostratigraphy and astrochronology studies in this Special Issue of *Palaeogeography, Palaeoclimatology, Palaeoecology*. For abbreviations, see caption to Table 1. (Zhang et al., 2019b; Xu et al., 2020; Du et al., 2020; Zhao et al., 2019; Liu et al., 2017a,b; Xu et al., 2019; Peng et al., 2020; Qu et al., 2014; Chu et al., 2020; Zhu et al., 2019a,b; Zhang et al., 2019a; Liu et al., 2018; Zhang et al., 2020; Wu et al., 2017; Kametaka et al., 2009; Lu et al., 2019;Zhong et al., 2019b; Tang et al., 2017; Ma et al., 2019; Fang et al., 2020; Peng et al., 2009; Condon et al., 2005; Sui et al., 2019; McFadden et al., 2008; Condon et al., 2005); Deng et al., 2018

Table 2 -- Summary of cyclostratigraphy and astrochronology studies in this this Special Issue of *Palaeogeography, Palaeoclimatology, Palaeoecology*

#	Author (* =Corresp.), publication	Geologic System (Stage)	What was calibrated	Result	Location	Main studied facies; depos. environ., thickness; Age control	(1) Proxies; (2) Method	Main cycle for tuning (implied span of record); Other recorded cycles	Raw data provided?	(1) Associated paleontology or age control; (2) Other information
1	Rui Zhang et al. 2019b (Chunju Huang*), Palaeo-3, 530: 78-89.	Quaternary (Pleistocene)	Fluvial-fan cycles	Interglacials (max of short-eccentricity cycles) are coarser-grained; interpreted as increased runoff pulses and more chemical weathering.	Xinjiang, western Tarim Basin (KT11 borehole, Kashgar region), 39.294°N, 76.539°E	Sand to clay, middle Kashgar fluvial fan, 800 m; ESR (electron spin resonance) dates and magnetostratigraphy	(1) GR, MS, Rb/Sr; (2) MTM spectral analysis, band-pass filters	100-kyr e (ca. 70 m) (11 cycles, 1.13 Myr); O (ca. 30 m), P (ca. 14 m)	Suppl. Excel tables (97600 GR levels, 1600 MS levels, Geochem)	
2	Yang Zhang et al. 2019 (James Ogg*), Palaeo-3, 527: 118-132.	Neogene-Quaternary (Pliocene-Pleistocene)	Continental slope depositional history	Coarser siliclastic influxes at end of glacials; Slow sed-accum. rates during warm intervals (mid-Plioc., early Gelasian, early Calabrian, and at ca. 0.6 Ma).	North margin of South China Sea (SE of Hong Kong, IODP Hole U1499A), 18.409°N, 115.860°E	Bioclastic clay with clayey silt layers, 333 m; Magnetostratigraphy (that study) and Plio-Pleist polarity scale, calcareous nannofossils	(1) GR, Paleomag; (2) MTM spectral analysis, eCOCO for sed-accum. rates, evolutive spectra, band-pass filters, tuning	405-kyr E (ca. 33 m); e (ca. 8 m), P (ca. 1.5 m)	Suppl. Excel tables (2700 GR levels, full Pmag 220 samples)	
3	Yingchao Xu et al., 2020 (Zhongmin Zhu*), Palaeo-3, 541: 109532.	Neogene-Quaternary (Pliocene-Pleistocene)	Delta, borehole	0 to 3.1 Ma chronology for Yangtze River delta location.	Jiangsu Prov. (north flank Yangtze River delta, Nantong City; core ZKA2); 32.563°N, 121.077°E	Alluvial-fluvial sand-silt-clay, then upper intertidal silty-clay; 295 m; Magnetostrat (same paper)	(1) GR, MS; (2) MTM, spectral analysis, band-pass filters	405-kyr E (ca. 40 m) (12 cycles, 4.7 Myr), then enhanced tuning with 100-kyr e (ca. 13 m); P (ca. 2.5 m)	Suppl. Excel tables (5880 GR levels; magnetric properties, etc.)	
4	Wei Du et al. 2020 (Youliang Ji*), Palaeo-3, 554, 109803.	Paleogene (Oligocene)	Lacustrine history	Semi-deep lake and fans 33.1-31.6 Ma, shallow-lake to 30.1 Ma, filling by fluvial plains to 25.5 Ma; plus ages for sand pulses (oil-gas reservoirs).	Hebei Prov., Bohai Bay Basin (Jizhong Depression, wells W33 and W62, 10 km E of Suning County), 38.42°N, 115.85°E	Oil shale (upper Mbr of Shahejie Fm, E. Olig., ca. 600 m). Mudstone to sandstone (Dongying Fm, Lt. Olig., ca. 800 m); Seismic correlation to wells with dated volcanics, magstrat, cyclostrat, and ostracod-algae-pollen assemblages. Tuning tied to base-Neogene reflector	(1) GR; (2) MTM spectral analysis, Evol. spectra, band-pass filters, tuning	405-kyr E (ca. 70 m) (24.5 cycles; 10.1 Myr); e (avg. ca. 20 m), O (avg. ca. 10 m), P (avg. ca. 5 m)	Suppl. Excel table (13000 GR levels well W33; 6000 well W62)	
5	Ke Zhao et al. 2019 (Xuebin Du*), Palaeo-3, 528: 35–49.	Paleogene (middle Eocene)	Lacustrine laminaa	Cycle-age control imply laminae are annual with Summer carbonate, Winter algal-organic clay.	east of Shandong Prov., southern Bohai Bay Basin (NY1 borehole, Dongying Depression), 37.3°N, 118.4°E	Carbonate-clay couplets, Shahejie Formation (upper Es4 and lower Es3 units), 350 m; Previous cyclostrat study (Liu et al., 2017) on Shahejie Fm members; base Es4u 45.4 Ma, top Es3l 42.2 Ma	(1) GR for cycles; Geochem for laminae; (2) [Acycle] MTM spectra analysis, Evol. spectra, band pass, tuning	405-kyr E (40 m, 8 cycles, ca. 3.2 Myr); e (8 m), O (3.7 m), P (2.2 m)	**No**	(1) Liu, Z.H., et al, 2017, *Palaeo-3*, **510:** 78-92.
6	Ke Xu et al. 2019 (Honghan Chen* & Chunju Huang*), Palaeo-3, 532: 109253.	Paleogene (Paleocene-Oligocene)	Terrestrial basin history correlated to Pacific convergence rates	46-Myr cycle-scale for entire Paleogene and latest Cretaceous. Rifting episodes at 54, 50 and 33 Ma.	Henan-Hubei border, Nanxing Basin (central Biyang Depression, ca. 30 km SW of Biyang, BS1 (deepest well in central China) and B270 well), ca. 32.6°N, 113.2°E	Paleocene floodplain of siliciclastics and mudstone; Eoc-Olig lacustrine (closed-lake) claystone, oil shale and dolomite. 6000 m and 2300 m; Green algae (Characeae), Ostracods, Spore-pollen. Astronomical tuning is relative to base-Neogene 23.03 Ma.	(1) GR for cycles; Geochem for laminae; (2) [ACycle] MTM spectral analysis, evolutive spectra, eCOCO for sed-accum rates, peak-ratios, bandpass filtering, tuning	405-kyr E (avg. ca. 60 m); e (avg. ca. 15 m), O (avg. ca. 5 m), P (avg. ca. 3 m); plus ca. 2 Myr. Modulation cycles in TOC of ca. 1.2 Myr.	Suppl. Excel tables (GR - 32000 levels for each well , TOC, XRF)	(2) Analyses done in different intervals due to changing sed-accum. rates
7	Cheng Peng et al. 2020 (Changchun Zou*), Palaeo-3, 555, 109858.	Cretaceous (Cenomanian-Coniacian)	Fluvial-delta and lacustrine deposits	Quantou Fm (5.5 Myr span) has long-eccentricity-driven influxes of fluvial siltstone.	Heilongjiang Prov., Songliao Basin (SK-2 well, Anda City), ca. 46.241°N, 125.363°E	Mudstone to siltstone (fluvial-deltaic, Quantou Fm., 860 m studies), mudstone and oil shale (lacustrine, Qingshankou Fm, 300 m studied); Correlation to SK-1 borehole radioisotopic dating and biostratigraphy for the same formations.	(1) Resistivity imaging logs, Mud-logging; (2) [Acycle] MTM spectral analysis, Evol. spectra, COCO sed-accum. rate, band-pass filters, tuning	405-kyr E (ca. 14 cycles of avg. 70 m in Qantou Fmr; ca. 13 cycles of 22 m in Qingshankou Fm) implies ca. 5.5 Myr each; e, O, P	**No**	
8	Yongxiang Li* et al., 2020, Palaeo-3, 538, 109465.	Cretaceous (Cenomanian-Turonian)	Marine carbonates. Cenom-Turon Oceanic Anoxic Event 2 (OAE2)	Obliquity in this interval drove tropical-subtropical climate, in addition to at high-latitude.	southern Tibet (Gongzha section, ca. 40 km W of Tingri), 28.8°N, 86.6°E	Limestone and marly limestone, outer-shelf, 76 m; Planktonic foraminifer zones, and carbon-isotope OAE2 excursion in the section	(1) Magnetic proxy for redox (log of HIRM/MS); 696 cubes; (2) [Acycle, eCOCO] MTM spectral analysis, Evol. spectra, band-pass filters, tuning	100-kyr e (4.4 m); but no direct tuning; O (ca. 1.6 m), P (ca. 1.0 m)	Suppl. Excel table (Rock Mag proxies; 696 levels)	
9	Wei Liu et al. 2020 (Huaichun Wu*), Palaeo-3, 541, 109555.	Cretaceous (lower)	Fluvial-alluvial basin fill	Relative timing of alluvial-lacustrine dominance. Coal-rich horizons at 100-kyr intervals in upper part.	west Heilongjiang Prov., Songliao Basin (50 km SE of Daqing, SS4 borehole), 46.3°N, 125.9°E	Mudstone to conglomerate with some coal horizons in upper part, Shahezi Fm, 836 m; Ar/Ar and K/Ar dating suggest Shahezi Fm spans 140 to 130 Ma	(1) GR; Litho-facies rank; (2) MTM spectral analysis, evolutive spectra, peak-ratio, band-pass filters, tuning	405-kyr E (avg. ca. 35 m) (ca. 27.5 cycles total; 11.4 Myr); e (avg. ca. 8 m), O (avg. ca. 3 m), P (avg. ca. 1.5 m) -- Wavelengths shift among intervals	Suppl. Excel table (Lithology rank, GR) -- But link Is broken	(1) Qu et al., 2014, Earth Sci. Front., 21: 234-250. (2) Analyses done in segments due to changes in sed-accum. rates
10	Runjian Chu et al., 2020 (Huaichun Wu* & Rukai Zhu*), Palaeo-3, 541, 109542.	Triassic (lower Ladinian)	Lacustrine organic-carbon-rich source rock	Chang 7 black shale spans ca. 3 Myr; Precession modulated the anoxic conditions.	Shaanxi Prov. Ordos Basin (Yaoqu section outcrops, Yishi, Taoqu, Tongchuan district), 35.17°N, 108.87°E	Black shale in Chang 7 Mbr, middle of Yanchang Fm; 11.6 m; ID-TIMS U-Pb of 241.56 ±0.09 Ma Base and 241.06 ±0.12 Ma Top of black-shale in same section; plants, palynology, ostracods	(1) MS, GR, Geochem, TOC; (2) MTM spectral analysis, band-pass filters	100-kyr e (ca. 4 m) and 20-kyr P (ca. 0.8 m); semi-precession (01 kyr; 0.4 m)	Suppl. Excel table -- But link Is broken	(1) Zhu, R.K., et al., 2019, Acta Geol. Sinica, 93:1823-1834.

(continued on next page)

Table 2 (*continued*)

#	Author (* =Corresp.), publication	Geologic System (Stage)	What was calibrated	Result	Location	Main studied facies; depos. environ., thickness; Age control	(1) Proxies; (2) Method	Main cycle for tuning (implied span of record); Other recorded cycles	Raw data provided?	(1) Associated paleontology or age control; (2) Other information
11	Rui Zhang et al., 2019a (Zhijun Jin* & Quanyou Liu*), Palaeo-3, 528, 87-98.	Triassic (lower Ladinian)	Lacustrine organic-carbon-rich source rock	Chang 7 Mbr spans ca. 5 Myr; and 20.5-m oil shale is 1.7 Myr.	Shaanxi Prov. Ordos Basin (well Y1011, Zhidan County)	Dark silty shale and oil shale with ash beds; Chang 7 Mbr, middle of Yanchang Fm; 65.9 m; Flora, spore-pollen assemblages, U-Pb dates from coeval intervals elsewhere	(1) MS; (2) [Acycle, eCOCO], Ash-free MTM, ASM sed-accum rate, Evol. spectra, band-pass filters, visual tuning	405-kyr E (ave. 5.4 m; 12.5 cycles, 5 Myr); e (avg. 1.6 m), O (0.5 m), P (avg. 0.27 m)	Suppl. Excel table (1256 MS levels)	(1) U-Pb: Liu, J., et al., 2018, Vert. Pal. Asiat. 56: 16-24; Deng, S.H., et al, 2018, Sci. China Earth Sci. 61: 1419-1439.
12	Tan Zhang et al., 2020 (Tailing Fan*), Palaeo-3, 539, 109493.	Triassic (Olenekian)	Terrestrial fan-delta; 2 borehole wells	Baikouquan Fm. spans 2 Myr.	Xinjiang Prov., Junggar Basin (Huangyangquan fan on the slope of the Mahu Sag at the northwestern margin), ca. 44.3°N, 85°E	Conglomerate to siltstone, Baikouquan Fm., 150-160m, fan-delta; Pollen - spore assemblages	(1) GR; (2) [Acycle, eCOCO] MTM spectral analysis, Evol. spectra, band-pass filters, tuning	405-kyr E (ca. 33 m; 5 cycles; 2.0 ±0.1 Myr); e, O	Excel ?; Under embargo until 26Nov2020.	
13	Xu Yao* and Linda Hinnov, 2019, Palaeo-3,	Permian (Roadian-Capitanian)	Deep-marine chert	Base-Roadian to mid-Capitanian spans 5.4 Myr (Wordian 3.7 Myr). Radiolarite sed-accum. rate of ca. 4 m/Myr. New couplet-cycle analysis method.	Anhui Prov. (Chaohu City, Anmenkou section), 31.6°N, 117.8°E	Radiolarian chert and mudstone alternations, outer-shelf (Gufeng Fm.), 28 m (19m studied); ID-TIMS U-Pb 271.04±0.1 Ma at 3m below base Gufeng Fm; conodont (base of section), then Radiolarian assemblages.	(1) Chert-clay couplet coding; (2) MTM spectral analysis, Evol. spectra,Bandpass filtering, Obliq-Prec tuning target of 6-Myr span, scaling to 270 Ma as base of Gufeng Fm	35-kyr Obliq (ca. 15 cm); P (ca. 9 cm), 405-kyr E (ca. 1.6 m)	Suppl. Excel table (thicknesses 175 couplets)	(1) U-Pb: Wu, Q., et al., 2017, Palaeo-3, 466: 351-372; Radiolaria: Kametaka et al., 2009, Island Arc, 18: 108-125.
14	Yangbo Lu et al., 2019 (Chunju Huang* and Shu Jiang*), Palaeo-3, 526: 96-109.	Ordovician (u. Katian, Hirnantian)	Marine shale. Graptolite zones and glacial sea-level curve	Lt. Katian: *Di. complanatus* (upper), *Di complexus, Para. pacificus*, = 0.6, 0.8, 1.8 Myr; Hirnantian (1.74 ±0.4 Myr total): Nor. etraordinarius, Per. persculptus = 1.2, 0.5 Myr	west Hubei Prov., (EHD1 borehole, Yichang); 30.102°N, 110.137°E (120 km NW of Hirnantian GSSP)	Marine black siliceous shale with ash beds; Wufeng Formation and the lowermost Longmaxi formations; 9.1 m; Correlation of lithologic units to Wangjiawan section outcrop with graptolite zones	(1) XRF (Fe signal) at 1-cm intervals; (2) ash-free series; MTM spectral analysis,evol. spectra, eCOCO, band pass filters, tuning	405 kyr E (0.75 m) for tuning (12.25 cycles; 5.0 Myr); e (avg. 0.3 m), O (avg. 6 cm), P (avg. 4 cm);obliquity-modulations of ca. 1.2 Myr (2.2 m);	**No**	
15	Yangyang Zhong et al., 2019b (Huaichun Wu*), Palaeo-3, 540: 109520.	Ordovician (u. Katian-Hirnantian)	Marine shale. International geologic stage (Hirnantian); Graptolite zones	Hirnantian Stage 1.26 myr; Late Katian graptolite zones: *D. complexus* (1.3 *myr), P. pacificus* (1.8 myr). Length of day = 22.4 ±0.1 hr	NE Yunnan Prov. (Wanhe roadcut; 27.76°N, 103.48°E)	Calcareous claystone; deep-water; 48.5 m; Graptolites (projected)	(1) MS; (2) MTM spectral analysis, Evol. spectra, band-pass filters, tuning	405 kyr E (avg. 3 m) for tuning (18 cycles; 7.37 Myr); e (avg. 0.9 m), O (avg.0.25 m) , P (avg. 0.15 m). Modulations of 1.3 Myr (obl.), and 2.4 and 1.4 Myr (ecc.)	Suppl. Excel table (2677 pts)	(1) Graptolite zones projected from Tang, P., et al., 2017, J. Strat., 41, 119–133.
16	Xueying Ma, et al., 2020 (Shenghui Deng*), Palaeo-3, in review.	Ordovician (Sandbian-lower Katian)	Marine carbonte. Delta13C excursion (GICE)	Sandbian > 6.4 Myr. Latest Sandbian-early Katian Positive 13-C excursion ("GICE") spans ca. 4 Myr. Pagoda Lms Fm spans 5.5 to 6 Myr.	NE Sichuan Prov. (Qiaoting, Bazhong, 32.46°N, 106.89°E), SE Sichuan (Xikou, Huaying, 30.16°N, 106.69°E); Chongqing (Sanquanzhen Nanchuan, 29.14°N, 107.19°E), N Guizhou Prov. (Liangcun, Xishui 28.46°N, 106.35°E)	Limestone; Pagoda Limestone, 32 m; Yangtze Platform; Conodonts	(1) MS; (2) MTM, Evol. spectra, band-pass filters, tuning	405-kyr E (ca. 2 m) for tuning (33 cycles lower Sandbian through top of e. Katian Pagoda Lms; 13.6 Myr); e, O, P	**?**	(1) Ma, X.Y., et al., 2019a, J. Strat., 43: 1-10; Wang, Z.H., et al., 2018, Acta Micro. Sinica, 35: 13-29; and other publ.; (2) GICE excursion is more complete in the southern sections on the Yangtze Platform.
17	Kunyuan Ma et al., 2019 (Yiming Gong*), Palaeo-3, 528: 272-287.	Ordovician (Floian)	Marine carbonate. International geologic stage; Conodont zones	Floian 7.08 ±0.4 Myr; Conodont zones: *S. bilobatus* 1.0 Myr, *S. extensus* 5.1 Myr, *O. communis* 0.2 Myr, *O. evae* 0.8 Myr, and *B. triangularis* 0.2 Myr.	W Hubei Prov. (Yichang, Huanghuachang GSSP for Dapingian 30.86°N, 110.37°E) and Hebei Prov. (Liangjiashan section; 40.10°N, 119.59°E)	Limestones, 41 m and 112 m, both shallow shelf; Conodonts	(1) XRF-Ca and Fe/Ca; (2) MTM spectral analysis, Evol. spectra, band-pass filters, tuning	405-kyr E (ca. 5 m Huanghuachang; ca. 7 m Liangjiashan) for tuning (totals of 7.5 and 18.5 cycles; 3.0 and 7.0 Myr); e, O, p. Modulations of 1.0 and 1.9 Myr.	Suppl. Excel table (1033 and 514 Ca-value horizons for the 2 sections)	(1) Liangjiashan section -- conodont study is part of the cyclostrat paper. Huanghauchang GSSP -- Wang, X.F., et al., 2009, *Episodes*, **32:** 96–113. (2) Cyclostratigraphy analysis required removing distortions by storm beds.
18	Jichuang Fang et al., 2020 (Huaichun Wu*), Palaeo-3, 540: 109530.	Cambrian (Drumian-Guzhangian)	Marine carbonate. Trilobite zones	Late Drumian trilobites zones: G. nathorsti 0.52 Myr, L. armata 0.15 Myr. base-Guzhangian: L. laevigata >0.7 Myr. Length of day = 21.6 ±0.2 hr.	Hunan Prov. (Guzhang, Luoyixi (formerly Wangcun) roadcut = Guzhangian GSSP; 28.72°N, 109.97°E)	Clayey limestones, mid-depth slope, 87 m; Trilobites	(1) MS, 13C; (2) MTM spectral analysis, Evol. spectra, band-pass filters, tuning	405-kyr E (ca. 25 m) for tuning (3.5 cycles; 1.4 Myr); e (avg. 6.6 m), O (avg. 1.96 m), P (avg. 1.13 m)	Suppl. Excel table (MS 4340 pts, Delta13C)	(1) Peng, S.C., et al., 2009, Episodes 32, 41–55.
19	Zheng Gong* et al., 2019, Palaeo-3, 528: 232-246.	Ediacaran	Marine carbonate. Shuram negative carbon-isotope excursion	Shuram CIE onset at ca. 560 Ma (ca. 20 Myr after Gaskiers Glaciation), and spanned ca. 9 Myr. Magnetostrat had been overprinted in Late Triassic.	Guizhou Prov. (Huanglianba section, Songtao county); 29.191°N, 109.266°E	Dolomite and black shale; margin-slope; Doushantuo Fm., 75 m (cyclostrat on 4-m carbonate interval at 53-57 m); U-Pb date of 551.1 ±0.7 Ma just below top of same formation elsewhere	(1) MS; (2) MTM spectral analysis, ASM for optimal sed-accum rate; ratio fit; band-pass	95-kyr e (0.8 m); 4-m section spans ca. 0.5 Myr; O (30 cm); P (18 and 14 cm); Sub-Milankovitch of ca. 6 kyr	Suppl. Excel (200 MS levels; Pmag; 13C, etc.)	(1) U-Pb: Condon et al., 2005, China Sci., 308: 95-98.
20	Yu Sui et al., 2019 (Chunju Huang*), Palaeo-3, 532: 109273.	Ediacaran	Marine carbonate. Shuram/Wonoka negative 13C excursion (upper Dushantou Fm)	Shuram CIE onset at ca. 571 Ma, and spanned ca. 20 Myr.	W Hubei Prov. (5 km east of Three Gorges Dam, Jiulongwan roadcut; 30.80°N, 111.06°E)	Dolomite and black shale; margin-slope; Doushantuo Fm., 154 m (upper 85 m in this study); U-Pb dates near base and top of this section; 13C excursions; U-Pb dates near base and top of this section.	(1) Fe, Si and Ca in XRF (4226 levels); (2) MTM spectral analysis, Evol. spectra, band-pass filters, tuning	405-kyr E (avg. 1.6 m) for tuning (73 cycles; 29.7 Myr); e (avg. 0.5 m), O (avg. 0.12 m), P (avg. 0.06 m), Modulations of eccentricity (ca. 2.2 Myr)	**No**	(1) McFadden et al., 2008, PNAS, 105: 3197-3203; Condon et al., 2005, Science, 308: 95-98; (2) The analysis was done in 4 intervals due sediment-accumulation rate changes

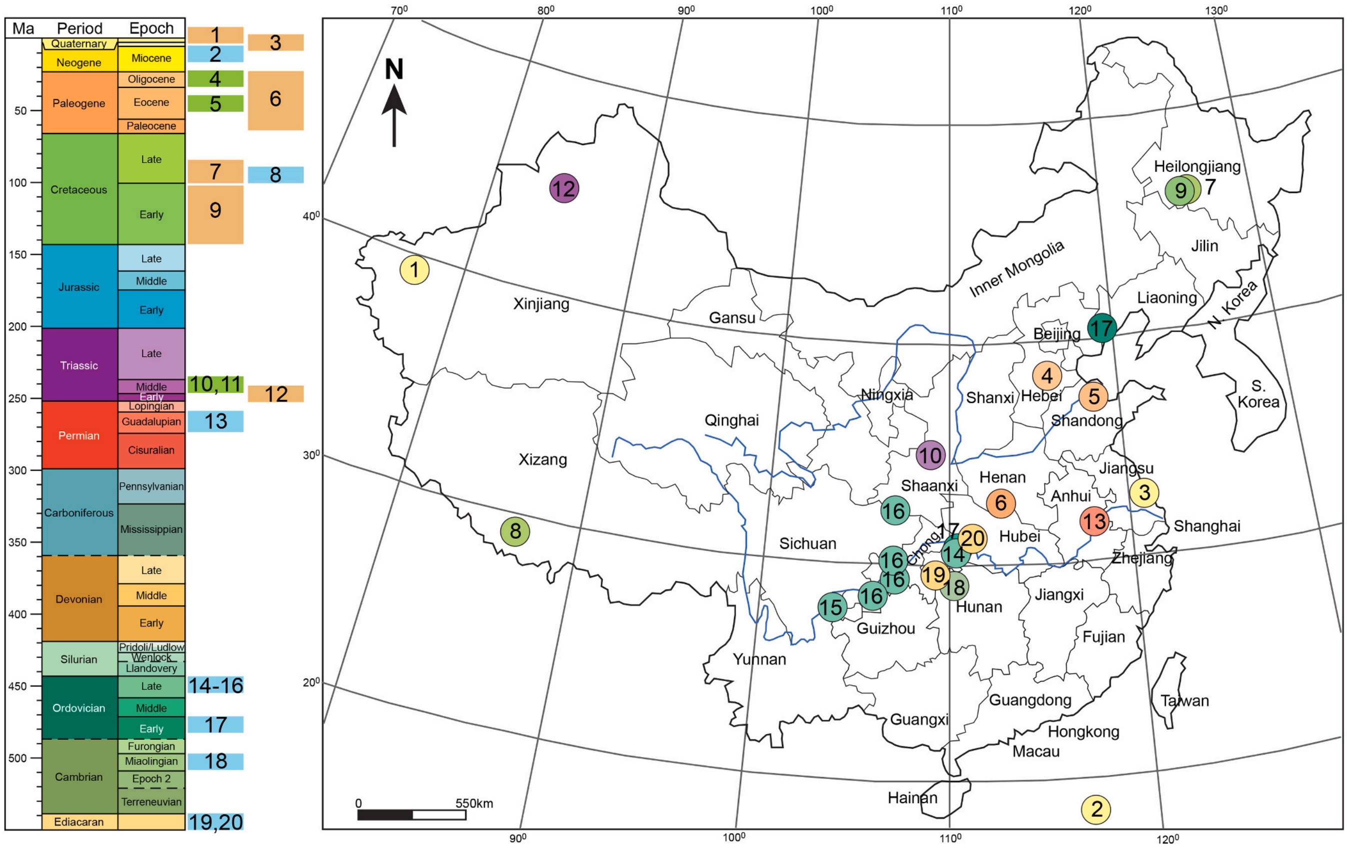

Fig. 2. Location of cyclostratigraphy studies in China in this Special Issue of *Palaeogeography, Palaeoclimatology, Palaeoecology*. The color of each location dot is the same as the color of the geologic epoch. Coloring of the bars for the span of each study (next to the geologic time scale) indicates the general depositional setting (blue = marine, green = lacustrine, tan = other terrestrial). For details on each study, see the corresponding number in Table 2. (For interpretation of the references to color in this figure legend, the reader is referred to the web version of this article.)

5. General methods

5.1. Paleoclimatic proxies

Cyclostratigraphy is dependent on recognizing orbital cycles in climatically sensitive physical, chemical or biological proxies. In order to understand how paleoclimatic proxies can record astronomical signals, cyclostratigraphers need to know how the paleoclimate changed in response to astronomically forced insolation variations, how these paleoclimatic variations influenced climate-sensitive components of the sedimentary record, and how the recording of these climate-sensitive components in the resulting deposits are linked to different proxies. Due to the Earth's rotation and its orbit around the Sun, the solar irradiance has strong daily, seasonal and annual cycles. Non-linear mechanisms rectify the seasonal modulation, thereby enhancing precessional-period and other Milankovitch cycle variability (Huybers and Wunsch, 2003). This seasonal-scale climatic transformation of the modulation of insolation forcing can amplify the astronomical frequencies and subsequently be preserved in stratigraphic records (Hinnov, 2018).

Paleoclimate proxies of widespread use in cyclostratigraphy include color, lithology, stable isotopes, rock magnetism, paleontology, gamma ray logs, elemental geochemistry, and organic carbon content (e.g., Hinnov, 2013; Li et al., 2019a). In this Special Issue, many types of paleoclimatic proxies were measured as a basis for analysis by spectral methods. Physical proxies include lithologic characteristics (i.e., chert-clay couplet coding, bed bundling, color), borehole well logs (i.e., resistivity, and natural gamma ray (GR) of Th, K and U contents), and magnetic parameters (i.e., magnetic susceptibility (MS), anhysteretic remanent magnetization (ARM), and hard Isothermal remanent magnetization/magnetic susceptibility (HIRM/χ)). Geochemical proxies include total organic carbon (TOC), carbon isotopes ($\delta^{13}C$), and XRF scanning data of elemental concentrations and ratios (Fe, Ca, Si, Ti, Rb/Sr, Sr/Al, Zr/Al, V/Cr, Ni/Ti, Cu/Ti, Fe/Ca).

In terrestrial or lacustrine settings, variations in some of these paleoclimate proxies are responses to astronomical-forced insolation changes in weathering, precipitation and temperature. In marine depositional settings, some of these paleoclimate proxies are records of variations in the relative productivity of carbonate organisms and variable fluxes of sediments derived from continental weathering and runoff (Li et al., 2019a).

5.2. Spectral analysis

Cyclostratigraphy requires the detection and separation of astronomical signals in paleoclimate proxy data (Hinnov and Hilgen, 2012). The most common procedures involve Fourier analysis of the proxy data to establish the frequency distribution of variance. High variance within a relatively narrow band of frequencies (i.e. spectral peaks) are used to identify likely cyclic signals within the dataset that represent the astronomical forcing. These spectral analysis methods are designed primarily to isolate signals in evenly-spaced time series. In contrast, proxy data measured through a stratigraphic record are in height/depth. Therefore, depending upon the type of deposit, well-defined, rapidly deposited event beds such as debris flows or turbidites are removed from the records. Methods such as evolutive harmonic analysis (EHA) and correlation coefficient (COCO) analysis (Meyers et al., 2001; Li et al., 2018b, 2019b) can be performed to identify temporal changes in the potential dominant cyclic frequencies preserved in stratigraphic sections, to reconstruct variations in sedimentation rates, and to select a suite of subintervals to analyze separately using spectral analysis.

Associated methods of time-series analysis of paleoclimate proxies employed in cyclostratigraphy include interpolation, integral-sampling, smoothing, detrending, filtering, and demodulation, correlation and tuning (Hinnov and Ogg, 2007). Common software for such signal processing includes *KaleidaGraph* 4.0, *Analyseries* 2.0.8, and *Acycle* 2.0. In this Special Issue, most studies utilize the multi-taper method (MTM) of spectral analysis, which offers high-resolution and statistical estimates that are independent of spectral power (Ghil et al., 2002). The MTM method can provide a well-resolved spectrum of variance within a dataset, allowing clear distinction of peaks even with small amplitude oscillations. The results are often more optimized than those based on other, more-classical spectral methods (Thomson, 1982). The statistical significance of spectral peaks, and thus whether they are likely to have been caused by astronomical cycles or perhaps relate to some random process instead, can be determined by establishing by how much the peak exceeds the expected background red-noise spectrum for an absence of cycles (e.g., Mann and Lees, 1996).

Most studies in this Special Issue also apply evolutionary spectral methods in order to visualize the time-frequency landscapes of the stratigraphic signals (e.g., Sui et al., 2019; Xu et al., 2019; Zhang et al., 2019b). Such analyses can provide important information that guide recognition of Milankovitch cycles through a section, as well as track variable sedimentation rates and the presence of hiatuses.

5.3. Astronomical tuning and construction of floating astronomical time scales

The main components of astronomical parameters are Earth's orbital cycles of precession, obliquity and eccentricity and their long-term modulation cycles. As noted above, Laskar et al. (1993, 2004, 2011) has progressively developed enhanced astronomical solutions (called La1993, La 2004, and La 2011, respectively) that now span from 250 Myr in the past to 250 Myr in the future. These numerical solutions provide an important astronomical time scale target and comparator to cyclostratigraphic results. Tuning of cyclostratigraphically identified cycles in proxy data to the astronomical solution allows for the construction of calibrated timescales anchored in absolute time. However, even the most recent solution of La2011 becomes uncertain for the high-frequency components of precession and obliquity beyond 50 Myr into the past, making any time-calibration of paleoclimatic proxy data to the Astronomical Time Scale difficult. Many stratigraphic records of paleoclimatic proxy series (e.g., Mediterranean sapropel sedimentary records, marine oxygen isotope and carbon isotope data, natural gamma ray (GR) logs, magnetic susceptibility, core-scanning XRF data, etc.) in the Cenozoic can be directly tuned to astronomical targets such as 65°N summer insolation, obliquity and eccentricity solutions (Ding et al., 2002; Lourens et al., 2004; Hilgen et al., 2012; Lisiecki and Raymo, 2005; Zachos et al., 2001).

Looking "backwards" in geologic time, Earth's orbital precession and obliquity periods become shorter relative to the Present due a reduction of the Earth-Moon distance and tidal dissipation, which caused changes in Earth's rotation rate and shape (Laskar et al., 2004). Therefore, for cyclostratigraphic analysis of deposits older than 50 Ma, the stable 405-kyr long-eccentricity cycles have emerged as the most prominent and stable orbital oscillation (Hinnov, 2018). This 405-kyr long-eccentricity cycle is caused by the combined interactions of the large mass of Jupiter and the perihelia of Venus and Jupiter on the Earth's orbit. Therefore, most cyclostratigraphy studies of Mesozoic and Paleozoic sediments tune their paleoclimatic proxy series to the 405-kyr long-eccentricity cycle (Bao et al., 2018; Boulila et al., 2014; De Vleeschouwer et al., 2015; Fang et al., 2018; Grippo et al., 2004; Huang et al., 2010a, 2010b; Husson et al., 2011; Li et al., 2016a, 2016b, 2018a; Pas et al., 2018; Ruhl et al., 2016; Wu et al., 2013c).

The predominant frequencies in rhythmic sedimentary stratigraphic records are observed from the power spectra and evolutionary spectral analysis results of paleoclimate proxies. Based on the estimates of variable sedimentation rates from methods such as COCO and EHA analyses, it is possible to determine whether the 405-kyr long-eccentricity, ~100-kyr short-eccentricity, or obliquity cycles are the dominant orbital parameter in high-resolution paleoclimatic proxy series. these cycles become the tuning term to convert the depth-domain signals into the time-domain, thereby enabling the construction of an astronomically tuned time scale. If the stratigraphic record of interest has a calibration based on a radio-isotopically dated horizon, or if the tuned-record of magnetic polarity zones can be matched to the calibrated geomagnetic polarity time scales (or similar types of age-control), then it is possible to apply cyclostratigraphy to generate a precise age model at every level within a stratigraphic succession.

In this Special Issue, nearly every study resolves a dominant 405-kyr long-eccentricity cycle and utilizes this term to construct floating astronomically tuned time scales. However, in some cases where multiple Milankovitch signals were identified, the tuning made use of the ~100-kyr short eccentricity cycle or obliquity cycle. This was the case for Quaternary fluvial-lake deposits (Zhang et al., 2019b), Cretaceous outer-shelf marine carbonates (Li et al., 2020), Middle Triassic lacustrine deposits (Chu et al., 2020), middle Permian deep-marine chert-shale couplets (Yao and Hinnov, 2019), and an Ediacaran marine carbonate succession (Gong et al., 2019).

5.4. Some caveats and challenges

Even though astronomically induced climate signals can be recognized in nearly every depositional setting in terrestrial and marine environments, the preservation and fidelity of that signal in the geologic record are influenced by many other natural processes. Strata do not accumulate steadily, and interruptions or disruptions in sediment accumulation can result in "missing cycles", time-averaging (e.g. bioturbation), and unstable sediment accumulation rates. Tectonics can cause fault-displaced records within an outcrop or borehole, and distortion of some types of paleoclimate proxies can occur through redox processes or diagenesis. In dynamic settings such as terrestrial and shallow-marine environments, non-cyclic fluvial-delta lobe switching and facies migration can occur, obfuscating astronomical signals. Most spectral analysis methods and bandpass separation of frequencies implicitly assume a semi-stable and continuous signal in the proxy being analyzed.

As a consequence of these issues, it is important to verify the interpretations from spectral-analysis, bandpass and tuning methods. If the methods are applied to more than one type of proxy, does one obtain the same results? Are each of the assigned cycles visibly present in the proxy records, and ideally also seen as features in the outcrop? Can the same cycles be resolved in an independent coeval section from another part of the basin? These types of verification and testing procedures have enabled development of a reliable astronomically tuned time scale for the Cenozoic and portions of the Mesozoic-Paleozoic. However, it is common for a study to concentrate on only a single reference section (e.g., over a third of the studies summarized in Tables 1 and 2), and these studies therefore await future verification. Confirmation of features in multiple sections is an issue that applies not only to cyclostratigraphic analyses, but also to many studies of geochemical excursions, magnetic polarity patterns, and impact horizons, more than a few of which were initially reported only from a single reference section.

It is also important for all studies to publish/archive their raw data and exact location information, so that future techniques can be reapplied to these datasets. In compiling our summaries, it was disturbing how many important studies, both legacy and current, did not provide the supporting raw data in an accessible form or indicate the exact geographic location of the sections with precise *Google-Earth*-verified latitude-longitude coordinates.

5.5. Outlook

A recent international collaborative effort within the cyclostratigraphic community (The Cyclostratigraphy Intercomparison Project, CIP) has sought to lay a foundation for standardization, both in terms of approach and reporting (Sinnesael et al., 2019). The CIP workshops explored how different approaches adopted for cyclostratigraphic analysis by the community can lead to different results, and thus this community-led approach has the specific aim of developing best practice protocols. A key outcome of the CIP work was the finding that cyclostratigraphy is a trainable skill. The rapid emergence of cyclostratigraphy and timescale development in China speaks to the importance of unifying the discipline in a way that ensures optimal, reproducible results that will add data and value to the geologic time scale.

Of particular note is the recent development of new software tools; in particular the *Astrochron* package for R (Meyers, 2014) and the *Acycle* code written for Matlab (Li et al., 2019b). Both packages provide a complete set of ready-to-use tools for cyclostratigraphic analysis of proxy data. The use of these tools helps to ensure reproducibility, eases communication of results, and also guides new researchers in cyclostratigraphy. We note that all but 3 of the papers in this Special Issue utilized either the *Acycle* or the *Astrochron* package. This emphasizes the clear demand and acceptance for these tools. Moreover, 12 studies utilize the COCO correlation coefficient method for constraining sedimentation rates recently introduced by Li et al. (2018b), which is integrated into the *Acycle* code. Although all workers must be wary of adopting 'black box' approaches in the statistical treatment and analysis of data (i.e., where the tools are used but not fully understood), the provision of these tools to the community means that integration and understanding of results should ultimately improve.

6. Future applications

In the near future, it should be possible to compile a global composite of Paleozoic-Mesozoic reference sections for a complete record of the 405-kyr "metronome" relative to the Present that encompasses all major biozones and is constrained by radioisotopic dates. This will extend the current Cenozoic astronomically tuned scale back to the Ediacaran. Such a preliminary "proof-of-concept" synthesis with standardized statistical processing of numerous overlapping sections was accomplished for the entire Mesozoic by Huang (2018), and the major 405-kyr "cyclothems" in the late Carboniferous through early Permian await a direct calibration to an enhanced astronomical solution.

There is also the exciting possibility of augmenting these compilations with the so-called "grand cycles" that modulate the amplitudes of the 405-kyr long-eccentricity cycles (ca. 1 to 2 Myr periodicities) and of obliquity (ca. 1.2 Myr periodicity). Such very-long-term cycles can act as additional time-scale and correlation constraints. It has already been shown that these modulations appear to influence global Phanerozoic sea level (e.g., Boulila et al., 2018) and govern the relative importance of obliquity versus eccentricity-precession cycles within basins (e.g., Li et al., 2016b). Some of these very-long-period modulations have been observed in longer sedimentary records within China (see the column with "other recorded cycles" in Tables 1 and 2). With constraints from radio-isotopic dates, it may be possible to bridge current gaps in the Mesozoic astronomically tuned time scale to begin a direct calibration of portions of Paleozoic time.

In turn, a verified master 405-kyr metronome may help to resolve the existing systematic "external uncertainty" of about 0.3 Myr or greater on most pre-Cenozoic radioisotopic dates. The analytical precision on such dates is often better than 0.1 Myr, but the added external uncertainty is a result of uncertainties in decay constants and of currently used "standards".

Looking further back in time, there is the challenge of analyzing pre-Cryogenian cyclostratigraphic successions. China hosts thick Mesoproterozoic deposits that appear to have cyclic characteristics; but studies are inhibited by the current lack of horizons that can be dated by radioisotopic methods to constrain sediment accumulation rates and the true nature of the cycles. This will probably be the next major frontier in China-hosted cyclostratigraphic studies, and it opens the possibility of understanding climate change in the pre-Cryogenian world.

Declaration of Competing Interest

None.

Acknowledgements

We thank Prof. Thomas Algeo, senior editor of *Palaeogeography, Palaeoclimatology, Palaeoecology*, for inviting us to organize this Special Issue, as well as all of the contributing teams who shared their studies. The astrochronology summary table was partly enhanced by Huaichun Wu and Linda Hinnov, and we thank them for providing preprints of their 2020 publications. Gabi Ogg prepared the graphics for this overview. CJH was supported by the National Natural Science Foundation of China (No. 41772029) and the 111 Project of China (grant no. BP0820004). DBK acknowledges support from the National Recruitment Program for Young Professionals (P.R. China). Support for JGO at CUG-Wuhan was funded by the Overseas Distinguished Teacher Program of the Ministry of Education (MS2013ZGDZ[WH]028) and at Chengdu University of Technology by a visiting scholar fellowship (National Natural Science Foundation of China, No. 41672102, to Hou Mingcai).

References

Bai, S.L., 1995a. High-resolution Correlation, Milankovitch Cyclicity, and Nickel Events. Peking University Press, Beijing, pp. 62 [in Chinese].
Bai, S.L., 1995b. Milankovitch cyclicity and time scale of the Middle and Upper Devonian. Int. Geol. Rev. 37, 1109–1114. https://doi.org/10.1080/00206819509465442.
Bai, S.L., Jin, S.Y., Ning, Z.S., 1982. Devonian Biostratigraphy of Guangxi and Adjacent Area (in Chinese). Peking University Press, Beijing, pp. 203 [in Chinese].
Bai, S.L., Bai, Z.Q., Ma, X.P., Wang, D.R., Sun, Y.L., 1994. Devonian Events and Biostratigraphy of South China. Peking University Press, Beijing, pp. 348 in Chinese.
Bao, X.J., Zhang, S.H., Jiang, G.Q., Wu, H.C., Wang, X.Q., An, Z.Z., Yang, T.S., 2018. Cyclostratigraphic constraints on the duration of the Datangpo Formation and the onset age of the Nantuo (Marinoan) glaciation in South China. Earth Planet. Sci. Lett. 483, 52–63. https://doi.org/10.1016/j.epsl.2017.12.001.
Boulila, S., Galbrun, B., Huret, E., Hinnov, L.A., Rouget, I., Gardin, S., Bartolini, A., 2014. Astronomical calibration of the Toarcian Stage: implications for sequence stratigraphy and duration of the early Toarcian OAE. Earth Planet. Sci. Lett. 386, 98–111. https://doi.org/10.1016/j.epsl.2013.10.047.
Boulila, S., Laskar, J., Haq, B.U., Galbrun, B., Hara, N., 2018. Long-term cyclicities in Phanerozoic sea-level sedimentary record and their potential drivers. Glob. Planet. Chang. 165, 128–136. https://doi.org/10.1016/j.gloplacha.2018.03.004.
Chen, X., Zhang, Y.D., Bergström, S.M., Xu, H.G., 2006. Upper Darriwilian graptolite and conodont zonation in the global stratotype section of the Darriwilian stage (Ordovician) at Huangnitang, Changshan, Zhejiang, China. Palaeoworld 15, 150–170. https://doi.org/10.1016/j.palwor.2006.07.001.
Chen, X., Bergstöm, S.M., Zhang, Y.D., Goldman, D., Chen, Q., 2011. Upper Ordovician (Sandbian-Katian) graptolite and conodont zonation in the Yangtze region, China. Earth Environ. Sci. 101, 111–134. https://doi.org/10.1017/S1755691010009199.
Chen, X., Zhang, Y.D., Wang, Z.H., Goldman, D., Bergström, S.M., Fan, J.X., Finney, S.C., Chen, Q., 2015. Biostratigraphy. In: Chen, X., Zhang, Y.D., Goldman, D., Bergström, S.M., Finney, S.C. (Eds.), Darrivilian to Katian (Ordovician) Graptolites from Northwest China. Zhejiang University Press (also Elsevier, 2016), pp. 7–38 ISBN-13: 978-0128009734.
Chen, X., Chen, Q., Zhen, Y.Y., Wang, H.Y., Zhang, L.N., Zhang, J.P., Wang, W.H., Xiao, Z.H., 2018. Circumjacent distribution pattern of the Lungmachian graptolitic black shale (early Silurian) on the Yichang Uplift and its peripheral region. Sci. China Earth Sci. 61, 1195–1203. https://doi.org/10.1007/s11430-017-9222-x.
Chu, R.J., Wu, H.C., Zhu, R.K., Fang, Q., Deng, S.H., Cui, J.W., Yang, T.S., Li, H.Y., Cao, L.W., Zhang, S.H., 2020. Orbitally forced Triassic monsoon activity in the Tethys realm and its involved internal feedback. Palaeogeogr. Palaeoclimatol. Palaeoecol. 541https://doi.org/10.1016/j.palaeo.2019.109542. article #109542: 11 pp.
Condon, D., Zhu, M.Y., Bowring, S., Wang, W., Yang, A.H., Jin, Y.G., 2005. U-Pb ages from the Neoproterozoic Doushantuo Formation, China. Science 308, 95–98. https://doi.org/10.1126/science.1107765.
De Vleeschouwer, D., Boulvain, F., Da Silva, A.-C., Pas, D., Labaye, C., Claeys, P., 2015.

The astronomical calibration of the Givetian (Middle Devonian) timescale (Dinant Synclinorium, Belgium). In: Da Silva, A.C., Whalen, M.T., Hladil, J., Chadimova, L., Chen, D., Spassov, S., Boulvain, F., De Vleeschouwer, X. (Eds.), Magnetic Susceptibility Application: A Window onto Ancient Environments and Climatic Variations. 414. Geological Society Special Publications of London, pp. 245–256. https://doi.org/10.1144/SP414.3.
Deng, C.L., He, H.Y., Pan, Y.X., Zhu, R.X., 2013. Chronology of the terrestrial Upper Cretaceous in the Songliao Basin, northeast Asia. Palaeogeogr. Palaeoclimatol. Palaeoecol. 385, 44–54. https://doi.org/10.1016/j.palaeo.2012.07.028.
Deng, S.H., Lu, Y.Z., Luo, Z., Fan, R., Li, X., Zhao, Y., Ma, X.Y., Zhu, R.K., Cui, J.W., 2018. Subdivision and age of the Yanchang Formation and the Middle/Upper Triassic boundary in Ordos Basin, North China. Sci. China Earth Sci. 61, 1419–1439 https://doi. org/10.1007/s11430-017-9215-3.
Deng, C.J., Hao, Q.Z., Guo, Z.T., Zhu, R.X., 2019a. Quaternary integrative stratigraphy and timescale of China. Sci. China Earth Sci. 62, 324–348. https://doi.org/10.1007/s11430-017-9195-4.
Deng, T., Hou, S.K., Wang, S.Q., 2019b. Neogene integrative stratigraphy and timescale of China. Sci. China Earth Sci. 62, 310–323. https://doi.org/10.1007/s11430-017-9155-4.
Ding, Z.L., Yu, Z.W., Rutter, N.W., Liu, T.S., 1994. Towards an orbital time scale for Chinese loess deposits. Quat. Sci. Rev. 13, 39–70. https://doi.org/10.1016/0277-3791(94)90124-4.
Ding, Z.L., Derbyshire, E., Yang, S.L., Yu, Z.W., Xiong, S.F., Liu, T.S., 2002. Stacked 2.6-Ma grain size record from the Chinese loess based on five sections and correlation with the deep-sea $\delta^{18}O$ record. Paleoceanography 17 (3). https://doi.org/10.1029/2001PA000725. article #1033: 5-1 to 5-2.
Du, W., Ji, Y.L., Chen, G., Wu, H., Gao, C.L., Li, S.M., Zhang, Y., 2020. Cyclostratigraphy and astronomical tuning during the Oligocene in the Jizhong Depression, Bohai Bay Basin, northeastern China. Palaeogeogr. Palaeoclimatol. Palaeoecol. 554https://doi.org/10.1016/j.palaeo.2020.109803. article #109803: 14 pp.
Fang, Q., Jing, X.C., Deng, S.H., Wang, X.L., 2012. Roadian–Wuchiapingian conodont biostratigraphy at the Shangsi section, northern Sichuan. J. Stratigr. 36, 692–699 (in Chinese with English abstract).
Fang, Q., Wu, H.C., Hinnov, L.A., Jing, X.C., Wang, X.L., Jiang, Q.C., 2015. Geologic evidence for chaotic behavior of the planets and its constraints on the third-order eustatic sequences at the end of the late Paleozoic Ice Age. Palaeogeogr. Palaeoclimatol. Palaeoecol. 440, 848–859. https://doi.org/10.1016/j.palaeo.2015.10.014.
Fang, Q., Wu, H.C., Hinnov, L.A., Jing, X.C., Wang, X.L., Yang, T.S., Li, H.Y., Zhang, S.H., 2017. Astronomical cycles of Middle Permian Maokou Formation in South China and their implications for sequence stratigraphy and paleoclimate. Palaeogeogr. Palaeoclimatol. Palaeoecol. 474, 130–139. https://doi.org/10.1016/j.palaeo.2016.07.037.
Fang, Q., Wu, H.C., Wang, X.L., Yang, T.S., Li, H.Y., Zhang, S.H., 2018. Astronomical cycles in the Serpukhovian–Moscovian (Carboniferous) marine sequence, South China, and their implications for geochronology and icehouse dynamics. J. Asian Earth Sci. 156, 302–315. https://doi.org/10.1016/j.jseaes.2018.02.001.
Fang, Q., Wu, H.C., Wang, X.L., Yang, X.L., Li, H.Y., Zhang, S.H., 2019. An astronomically forced cooling event during the Middle Ordovician. Glob. Planet. Chang. 173, 96–108. https://doi.org/10.1016/j.gloplacha.2018.12.010.
Fang, J.C., Wu, H.C., Fang, Q., Shi, M.N., Zhang, S.H., Yang, T.S., Li, H.Y., Cao, L.W., 2020. Cyclostratigraphy of the global stratotype section and point (GSSP) of the basal Guzhangian Stage of the Cambrian Period. Palaeogeogr. Palaeoclimatol. Palaeoecol. 540https://doi.org/10.1016/j.palaeo.2019.109530. article #109530: 9 pp.
Ghil, M., Allen, M.R., Dettinger, M.D., Ide, K., Kondrashov, D., Mann, M.E., Robertson, A.W., Saunders, A., Tian, Y., Varadi, F., Yiou, P., 2002. Advanced spectral methods for climatic time series. Rev. Geophys. 40 (1) article #1003, 3-1–3-41. doi:10.1029/2000RG000092.
Gilbert, G.K., 1895. Sedimentary measurement of Cretaceous time. J. Geol. 3, 121–127.
Gong, Y.M., Li, B.H., Wang, C.Y., Wu, Y., 2001. Orbital cyclostratigraphy of the Devonian Frasnian–Famennian transition in South China. Palaeogeogr. Palaeoclimatol. Palaeoecol. 168, 237–248. https://doi.org/10.1016/S0031-0182(00)00257-1.
Gong, Y.M., Xu, R., Tang, Z.D., Li, B.H., 2005. The Upper Devonian orbital cyclostratigraphy and numerical dating conodont zones from Guangxi. South China. Sci. China Series D Earth Sci. 48, 32–41. https://doi.org/10.1360/03yd0025.
Gong, Z., Kodama, K.P., Li, Y.X., 2017. Rock magnetic cyclostratigraphy of the Doushantuo Formation, South China and its implications for the duration of the Shuram carbon isotope excursion. Precambrian Res. 289, 62–74. https://doi.org/10.1016/j.precamres.2016.12.002.
Gong, Z., Kodama, K.P., Li, Y.X., 2019. Paleomagnetism and rock magnetic cyclostratigraphy of the Ediacaran Doushantuo Formation, South China: Constraints on the remagnetization mechanism and the encoding process of Milankovitch cycles. Palaeogeogr. Palaeoclimatol. Palaeoecol. 528, 232–246. https://doi.org/10.1016/j.palaeo.2019.05.002.
Gradstein, F.M., Ogg, J.G., Schmitz, M.D., Ogg, G.M. (Eds.), 2020. The Geologic Time Scale 2020. 2 volumes Elsevier Publ (ca. 1400 pp.), in press. https://www.elsevier.com/books/geologic-time-scale-2020/gradstein/978-0-12-824360-2.
Grippo, A., Fischer, A.G., Hinnov, L.A., Herbert, T.D., Premoli Silva, I., 2004. Cyclostratigraphy and chronology of the Albian stage (Piobbico core, Italy). *In*: D'Argenio, B., Fischer, A.G., Premoli Silva, I., Weissert, H., and Ferreri, V. (eds.), *Cyclostratigraphy: Approaches and Case Histories*. SEPM Spec. Publ. 81, 57–81. https://doi.org/10.2110/pec.04.81.0057.
Hays, J.D., Imbrie, J., Shackleton, N.J., 1976. Variations in the Earth's orbit: Pacemaker of the Ice Ages. Science 194, 1121–1132. https://doi.org/10.1126/science.194.4270.1121.
He, H.Y., Deng, C.L., Wang, P.J., Pan, Y.X., Zhu, R.X., 2012. Toward age determination of the termination of the Cretaceous Normal Superchron. Geochem. Geophys. Geosyst. 13 article #Q02002: 20 pp. doi:10.1029/2011GC003901.
Heslop, D., Langereis, C.G., Dekkers, M.J., 2000. A new astronomical timescale for the loess deposits of Northern China. Earth Planet. Sci. Lett. 184, 125–139. https://doi.org/10.1016/S0012-821X(00)00324-1.
Hilgen, F.J., Lourens, L.J., Van Dam, J.A., 2012. Chapter 29: The Neogene Period. In: Gradstein, F.M., Ogg, J.G., Schmitz, M.D., Ogg, G.M. (Eds.), A Geologic Time Scale 2012. Elsevier, Amsterdam, pp. 923–978.
Hinnov, L.A., 2013. Cyclostratigraphy and its revolutionizing applications in the earth and planetary sciences. Geol. Soc. Am. Bull. 125, 1703–1734. https://doi.org/10.1130/B30934.1.
Hinnov, L.A., 2018. Chapter One - Cyclostratigraphy and astrochronology in 2018. *In*: Montenari, M. (ed.). Stratigr. Time Scales (Academic Press) 3, 1–80. https://doi.org/10.1016/bs.sats.2018.08.004.
Hinnov, L.A., Hilgen, F.J., 2012. Cyclostratigraphy and astrochronology. In: Gradstein, F.M., Ogg, J.G., Schmitz, M., Ogg, G.M. (Eds.), The Geologic Time Scale 2012. Elsevier, Amsterdam, pp. 63–83. https://doi.org/10.1016/B978-0-444-59425-9.00004-4.
Hinnov, L.A., Ogg, J.G., 2007. Cyclostratigraphy and the astronomical time scale. Stratigraphy 4, 239–251.
Hu, K.Y., Qi, Y.P., 2017. The Moscovian (Pennsylvanian) conodont genus *Swadelina* from Luodian, southern Guizhou, South China. Stratigraphy 14, 197–215. https://doi.org/10.29041/strat.14.1-4.197-215.
Huang, C.J., 2018. Chapter Two - Astronomical time scale for the Mesozoic. In: Montenari, M. (ed.). Stratigr. Time Scales (Academic Press) 3, 81–150. https://doi.org/10.1016/bs.sats.2018.08.005.
Huang, D., 2019. Jurassic integrative stratigraphy and timescale of China. Sci. China Earth Sci. 62, 223–255. https://doi.org/10.1007/s11430-017-9268-7.
Huang, C.J., Hinnov, L.A., Fischer, A.G., Grippo, A., Herbert, T., 2010a. Astronomical tuning of the Aptian stage from Italian reference sections. Geology 38, 899–902. https://doi.org/10.1130/G31177.1.
Huang, C.J., Hesselbo, S.P., Hinnov, L.A., 2010b. Astrochronology of the Late Jurassic Kimmeridge Clay (Dorset, England) and implications for Earth system processes. Earth Planet. Sci. Lett. 289, 242–255. https://doi.org/10.1016/j.epsl.2009.11.013.
Huang, C.J., Deng, S.H., Dong, S.S., Hinnov, L.A., Zhang, R., Wang, Z.X., Lu, Y.Z., Li, X., 2016. Astronomically forced cyclicity in the Late Ordovician-Early Silurian, Sichuan Basin, China. In: Geological Society of America Annual Meeting (Denver, Colo.), Paper 127-2, . https://gsa.confex.com/gsa/2016AM/webprogram/Paper283308.html.
Husson, D., Galbrun, B., Laskar, J., Hinnov, L.A., Locklair, R., 2011. Astronomical calibration of the Maastrichtian. Earth Planet. Sci. Lett. 305, 328–340.
Huybers, P., Wunsch, C., 2003. Rectification and precession signals in the climate system. Geophys. Res. Lett. 30 (19) #2011: 4 pp. doi:10.1029/2003GL017875.
Kametaka, M., Nagai, H., Zhu, S.Z., Takebe, M., 2009. Middle Permian radiolarians from Anmenkou, Chaohu, northeastern Yangtze Platform, China. Island Arc 18, 108–125. https://doi.org/10.1111/j.1440-1738.2008.00649.x.
Laskar, J., Joutel, F., Boudin, F., 1993. Orbital, precessional and insolation quantities for the Earth from -20 Myr to +10 Myr. Astron. Astrophys. 270, 522–533.
Laskar, J., Robutel, P., Joutel, J., Gastineau, M., Correia, A.C.M., Levrard, B., 2004. A numerical solution for the insolation quantities of the Earth. Astron. Astrophys. 428, 261–285. https://doi.org/10.1051/0004-6361:20041335.
Laskar, J., Fienga, A., Gastineau, M., Manche, H., 2011. La2010: A new orbital solution for the long term motion of the Earth. Astron. Astrophys. 532, A89. 15 pp. https://doi.org/10.1051/0004-6361/201116836.
Lehrmann, D.J., Stepchinski, L., Altiner, D., Orchard, M.J., Montgomery, P., Enos, P., Ellwood, B.B., Bowring, S.A., Ramezani, J., Wang, H.M., Wei, J.Y., Yu, M.Y., Griffiths, J.D., Minzoni, M., Schaal, E.K., Li, X.W., Meyer, K.M., Payne, J.L., 2015. An integrated biostratigraphy (conodonts and foraminifers) and chronostratigraphy (paleomagnetic reversals, magnetic susceptibility, elemental chemistry, carbon isotopes and geochronology) for the Permian–Upper Triassic strata of Guandao section, Nanpanjiang Basin, south China. J. Asian Earth Sci. 108, 117–135. https://doi.org/10.1016/j.jseaes.2015.04.030.
Li, R.F., Liu, B.P., Zhao, C.L., 1997. Correlation of Carboniferous depositional sequences on the Yangtze Plate with others on a global scale (in Chinese with English abstract). Acta Sedimentol. Sin. 15, 23–28. http://www.cjxb.ac.cn/EN/Y1997/V15/I3/23.
Li, S.Y., Tong, J.N., Liu, K.Y., Wang, F.J., Huo, Y.Y., 2007. The Lower Triassic cyclic deposition in Chaohu, Anhui Province, China. Palaeogeogr. Palaeoclimatol. Palaeoecol. 252, 188–199. https://doi.org/10.1016/j.palaeo.2006.11.043.
Li, H., Tong, J.N., Ren, J.B., Zhang, J.K., 2009. Early Triassic bivalve biostratigraphy and paleocommunities at Xiakou section in Xingshan, Hubei province. Earth Sci. (Journal of the China University of Geosciences) 34, 733–742. (In Chinese with English abstract). http://en.cnki.com.cn/Article_en/CJFDTOTAL-DQKX200905005.htm.
Li, M.S., Ogg, J.G., Zhang, Y., Huang, C.J., Hinnov, L.A., Chen, Z.Q., Zou, Z.Y., 2016a. Astronomical tuning of the end-Permian extinction and the Early Triassic Epoch of South China and Germany. Earth Planet. Sci. Lett. 441, 10–25. https://doi.org/10.1016/j.epsl.2016.02.017.
Li, M.S., Huang, C.J., Hinnov, L.A., Ogg, J.G., Chen, Z.-Q., Zhang, Y., 2016b. Obliquity-forced climate during the Early Triassic hothouse in China. Geology 44, 623–626. https://doi.org/10.1130/G37970.1.
Li, M.S., Zhang, Y., Huang, C.J., Ogg, J.G., Hinnov, L.A., Wang, Y.D., Zou, Z.Y., Li, L., 2017. Astronomical tuning and magnetostratigraphy of the Upper Triassic Xujiahe Fm. of South China and Newark Supergroup of North America: Implications for the Late Triassic time scale. Earth Planet. Sci. Lett. 475, 207–223. https://doi.org/10.1016/j.epsl.2017.07.015.
Li, M.S., Hinnov, L.A., Kump, L., 2019b. *Acycle*: Time-series analysis software for paleoclimate research and education. Comput. Geosci. 127, 12–22 [Available at

www.mingsongli.com/Acycle].
Li, M.S., Huang, C.J., Hinnov, L.A., Chen, W.Z., Ogg, J.G., Tian, W., 2018a. Astrochronology of the Anisian Stage (Middle Triassic) at the Guandao reference section, South China. Earth Planet. Sci. Lett. 482, 591–606. https://doi.org/10.1016/j.epsl.2017.11.042.
Li, M.S., Kump, L.R., Hinnov, L.A., Mann, M.E., 2018b. Tracking variable sedimentation rates and astronomical forcing in Phanerozoic paleoclimate proxy series with evolutionary correlation coefficients and hypothesis testing. Earth Planet. Sci. Lett. 501, 165–179. https://doi.org/10.1016/j.epsl.2018.08.041.
Li, M.S., Huang, C.J., Ogg, J.G., Zhang, Y., Hinnov, L.A., Wu, H.C., Chen, Z.Q., Zou, Z.Y., 2019a. Paleoclimate proxies for cyclostratigraphy: comparative analysis using a Lower Triassic marine section in South China. Earth Sci. Rev. 189, 125–146. https://doi.org/10.1016/j.earscirev.2019.01.011.
Li, Y.-X., Gill, B., Montañez, I.P., Ma, L.F., LeRoy, M., Kodama, K.P., 2020. Obliquity driven redox fluctuations during Cretaceous Oceanic Anoxic Event 2 (OAE2) revealed by a mineral magnetic proxy. Palaeogeogr. Palaeoclimatol. Palaeoecol. 538 article #109465: 10 pp. doi:10.1016/j.palaeo.2019.109465.
Lisiecki, L.E., Raymo, M.E., 2005. A Pliocene-Pleistocene stack of 57 globally distributed benthic $\delta^{18}O$ records. Paleoceanography 20 article #PA1003: 17 pp. doi:10.1029/2004PA001071.
Liu, Z.H., Huang, C.J., Algeo, T.J., Liu, H.M., Hao, Y.Q., Du, X.B., Lu, Y.C., Chen, P., Guo, L.Y., Peng, L., 2017a. High-resolution astrochronological record for the Paleocene-Oligocene (66–23 Ma) from the rapidly subsiding Bohai Bay Basin, northeastern China. Palaeogeogr. Palaeoclimatol. Palaeoecol. 510, 78–92. https://doi.org/10.1016/j.palaeo.2017.10.030.
Liu, Z., Liu, X.M., Huang, S.P., 2017b. Cyclostratigraphic analysis of magnetic records for orbital chronology of the Lower Cretaceous Xiagou Formation in Linze, northwestern China. Palaeogeogr. Palaeoclimatol. Palaeoecol. 481, 44–56. https://doi.org/10.1016/j.palaeo.2017.05.022.
Liu, J., Jahandar, R., Li, L., Shang, Q.H., Xu, G.H., Wang, Y.Q., Yang, J.S., 2018. High-precision temporal calibration of Middle Triassic vertebrate biostratigraphy: U-Pb zircon constraints for the *Sinokannemeyeria* Fauna and *Yonghesuchus*. Vertebrata PalAsiatica 56, 16–24. https://doi.org/10.19615/j.cnki.1000-3118.170808.
Liu, W., Wu, H.C., Hinnov, L.A., Baddouh, M., Wang, P.J., Gao, Y.F., Zhang, S.H., Yang, T.S., Li, H.Y., Wang, C.S., 2020. An 11 million-year-long record of astronomically forced fluvial-alluvial deposition and paleoclimate change in the Early Cretaceous Songliao synrift basin, China. Palaeogeogr. Palaeoclimatol. Palaeoecol. 541, 109555 article #109555: 13 pp. doi:10.1016/j.palaeo.2019.109555.
Lourens, L.J., Hilgen, F., Shackleton, N.J., Laskar, J., Wilson, D., 2004. The Neogene Period. In: Gradstein, F.M., Ogg, J.G., Smith, A. (Eds.), A Geologic Time Scale 2004. Cambridge University Press, Cambridge, UK, pp. 400–440.
Lu, H.Y., Liu, X.D., Zhang, F.Q., An, Z.S., Dodson, J., 1999. Astronomical calibration of loess-paleosol deposits at Luochuan, central Chinese Loess Plateau. Palaeogeogr. Palaeoclimatol. Palaeoecol. 154, 237–246. https://doi.org/10.1016/S0031-0182(99)00113-3.
Lu, Y.B., Huang, C.J., Jiang, S., Zhang, J.Y., Lu, Y.C., Liu, Y., 2019. Cyclic late Katian through Hirnantian glacioeustasy and its controls on the development of the organic-rich Wufeng and Longmaxi shales, South China. Palaeogeogr. Palaeoclimatol. Palaeoecol. 526, 96–109. https://doi.org/10.1016/j.palaeo.2019.04.012.
Ma, K.Y., Li, R.C., Gong, Y.M., 2016. Chemostratigraphy and cyclostratigraphy of the Ordovician Liangjiashan Section from Shimenzhai of Qinhuangdao in North China. Earth Sci. Front. 23 (6), 268–286.
Ma, K.Y., Li, R.C., Hinnov, L.A., Gong, Y.M., 2019. Conodont biostratigraphy and astronomical tuning of the Lower–Middle Ordovician Liangjiashan (North China) and Huanghuachang (South China) marine sections. Palaeogeogr. Palaeoclimatol. Palaeoecol. 528, 272–287. https://doi.org/10.1016/j.palaeo.2019.05.003.
Ma, X.Y., Lu, Y.Z., Zhong, L., Fan, R., Li, X., Deng, S.H., 2019a. Carbon isotope characteristics of the Ordovician Pagoda Formation at the Sanquan Section in Nanchuan, Chongqing and its correlation. J. Stratigr. 43 (1), 1–10 (in Chinese with English abstract).
Ma, X.Y., Fan, R., Lu, Y.Z., Luo, Z., Deng, S.H., Zhang, F., 2019b. Middle-Upper Ordovician conodont sequence and its geological significance in Nanchuan area, Chongqing. Acta Pet. Sin. 40 (5), 577–586 (in Chinese with English abstract).
Ma, X.Y., Deng, S.H., Lu, Y.Z., Wu, H.C., Luo, Z., 628 Fan, R., Li, X., Fang, Q., 2019c. Astrochronology of the Upper Ordovician Pagoda Formation, South China and its geological implications. Earth Sci. Front. 26 (2), 281–291.
Ma, K.Y., Hinnov, L.A., Zhang, X.S., Gong, Y.M., 2020a. Astronomical time calibration of the Upper Devonian Lali section, South China. Global Planet. Change 193https://doi.org/10.1016/j.gloplacha.2020.103267. article #103267: 12 pp.
Ma, X.Y., Ogg, J.G., Lu, Y.Z., Fan, R., Huang, C.J., Luo, Z., Deng, S.H., 2020b. Cyclostratigraphy of the Upper Ordovician Pagoda Formation, South China: Implications for the duration and correlation of the Guttenberg $\delta^{13}C$ excursion (GICE). Palaeogeogr. Palaeoclimatol. Palaeoecol In press.
Mann, M.E., Lees, J.M., 1996. Robust estimation of background noise and signal detection in climatic time series. Clim. Chang. 33, 409–445. https://doi.org/10.1007/BF00142586.
McFadden, K.F., Huang, J., Chu, X.L., Jiang, G.Q., Kaufman, A.J., Zhou, C.M., Yuan, X.L., Xiao, S.H., 2008. Pulsed oxidation and biological evolution in the Ediacaran Doushantuo Formation. Proc. Natl. Acad. Sci. USA 105 (9), 3197–3202. https://doi.org/10.1073/pnas.0708336105.
Mei, S.L., Jin, Y.G., Wardlaw, B.R., 1994. Succession of conodont zones from the Permian "Kuhfeng" formation, Xuanhan, Sichuan and its implication in global correlation. Acta Palaeontol. Sin. 33, 1–23 (in Chinese with English abstract).
Meyers, S.R., 2014. Astrochron: An R package for astrochronology. Available at. http://cran.r-project.org/package=astrochron.
Meyers, S.R., Sageman, B.B., Hinnov, L.A., 2001. Integrated quantitative stratigraphy of the Cenomanian-Turonian Bridge Creek Limestone member using evolutive harmonic analysis and stratigraphic modeling. J. Sediment. Res. 71, 628–644. https://doi.org/10.1306/012401710628.
Milankovitch, M., 1930. Mathematische Klimalehre und astronomische Theorie der Klimaschwankungen. In: Köppen, W., Geiger, R. (Eds.), Handbuch der Klimatologie, Bd. 1: Allgemeine Klimalehre. Borntraeger, Berlin.
Milankovitch, M., 1941. Kanon der Erdbestrahlung und seine Anwendung auf das Eiszeitenproblem. Académie royale serbe. Éditions speciales; 132 [vielm. 133]: XX, 633, Belgrad, 1941.
Mundil, R., Ludwig, K.R., Metcalfe, I., Renne, P.R., 2004. Age and timing of the Permian mass extinctions: U/Pb dating of closed-system zircons. Science 305, 1760–1763. https://doi.org/10.1126/science.1101012.
Ogg, J.G., Ogg, G.M., Gradstein, F.M., 2016. A Concise Geologic Time Scale 2016. Elsevier Publ, pp. 1–234.
Pas, D., Hinnov, L.A., Day, J., Kodama, K., Sinnesael, M., Liu, W., 2018. Cyclostratigraphic calibration of the Famennian Stage (Late Devonian, Illinois Basin, USA). Earth Planet. Sci. Lett. 488, 102–114. https://doi.org/10.1016/j.epsl.2018.02.010.
Peng, S.C., Babcock, L.E., Zuo, J.X., Lin, H.L., Zhu, X.J., Yang, X.F., Robison, R.A., Qi, Y.P., Bagnoli, G., Chen, Y., 2009. The Global boundary Stratotype Section and Point of the Guzhangian Stage (Cambrian) in the Wuling Mountains, northwestern Hunan, China. Episodes 32 (1), 41–55. https://doi.org/10.18814/epiiugs/2009/v32i1/006.
Peng, C., Zou, C.C., Zhang, S.X., Wu, H.C., Lu, Q.T., Hou, H.S., Wang, C.S., 2020. Astronomically forced variations in multiresolution resistivity logs of lower Upper Cretaceous (Cenomanian-Coniacian) terrestrial formations from the Songliao Basin, northeastern China. Palaeogeogr. Palaeoclimatol. Palaeoecol. 555https://doi.org/10.1016/j.palaeo.2020.109858. article #109858: 15 pp.
Qi, Y.P., Nemyrovska, T.I., Wang, X.D., Chen, J.T., Wang, Z.H., Lane, H.R., Richards, B.C., Hu, K.Y., Wang, Q.L., 2014. Late Visean–early Serpukhovian conodont succession at the Naqing (Nashui) section in Guizhou, South China. Geol. Mag. 151, 254–268. https://doi.org/10.1017/S001675681300071X.
Qie, W.K., Ma, X.P., Xu, H.H., Qiao, L., Liang, K., Guo, W., Song, J.J., Chen, B., Lu, J.F., 2019. Devonian integrative stratigraphy and timescale of China. Sci. China Earth Sci. 62, 112–134. https://doi.org/10.1007/s11430-017-9259-9.
Qu, X.J., Wang, P.J., Gao, Y.F., Wan, X.Q., 2014. Chronostratigraphy of Huoshiling Formation in the Songliao Basin, NE China: an overview. Earth Sci. Front. 21 (2), 234–250 (Chinese with English abstract).
Rong, J.Y., Wang, Y., Zhan, R.B., Fan, J.X., Huang, B., Tang, P., Li, Y., Zhang, X.L., Wu, R.C., Wang, G.X., Wei, X., 2019. Silurian integrative stratigraphy and timescale of China. Sci. China Earth Sci. 62, 89–111. https://doi.org/10.1007/s11430-017-9258-0.
Ross, C.A., Ross, J.R.P., 1988. Late Paleozoic transgressive-regressive deposition. In: Wilgus, C.K., Hastings, B.S., Posamentier, H., Van Wagoner, J., Ross, C.A., Kendall, C.G.S.C. (Eds.), Sea-level changes: An integrated approach. 42. SEPM Special Publication, pp. 227–247. https://doi.org/10.2110/pec.88.01.0227.
Ruhl, M., Hesselbo, S.P., Hinnov, L.A., Jenkyns, H.C., Xu, W.M., Storm, M., Riding, J., Minisini, D., Ullmann, C.U., Leng, M.J., 2016. Astronomical constraints on the duration of the Early Jurassic Pliensbachian stage and global climate fluctuations. Earth Planet. Sci. Lett. 455, 149–165. https://doi.org/10.1016/j.epsl.2016.08.038.
Rygel, M.C., Fielding, C.R., Frank, T.D., Birgenheier, L.P., 2008. The magnitude of Late Paleozoic glacioeustatic fluctuations: A synthesis. J. Sediment. Res. 78, 500–511. https://doi.org/10.2110/jsr.2008.058.
Shen, S.Z., Crowley, J.L., Wang, Y., Bowring, S.A., Erwin, D.H., Sadler, P.M., Cao, C.Q., Rothman, D.H., Henderson, C.M., Ramezani, J., Zhang, H., Shen, Y., Wang, X.D., Wang, W., Mu, L., Li, W.Z., Tang, Y.G., Liu, X.L., Liu, L.J., Zeng, Y., Jiang, Y.F., Jin, Y.G., 2011. Calibrating the end-Permian mass extinction. Science 334, 1367–1372. https://doi.org/10.1126/science.1213454.
Shen, S.Z., Zhang, H., Zhang, Y.C., Yuan, D.X., Chen, B., He, W.H., Mu, L., Lin, W., Wang, W.Q., Chen, J., Wu, Q., Cao, C.Q., Wang, Y., Wang, X.D., 2019. Permian integrative stratigraphy and timescale of China. Sci. China Earth Sci. 62, 154–188. https://doi.org/10.1007/s11430-017-9228-4.
Sinnesael, M., De Vleeschouwer, D., Zeeden, C., et al. (total of 31 authors), 2019. The Cyclostratigraphy Intercomparison Project (CIP): consistency, merits and pitfalls. Earth-Science Rev. 199 article #102965: 16 pp. doi:10.1016/j.earscirev.2019.102965.
Sui, Y., Huang, C.J., Zhang, R., Wang, Z.X., Ogg, J.G., Kemp, D.B., 2018. Astronomical time scale for the lower Doushantuo Formation of early Ediacaran, South China. Sci. Bull. 63, 1485–1494. https://doi.org/10.1016/j.scib.2018.10.010.
Sui, Y., Huang, C.J., Zhang, R., Wang, Z.X., Ogg, J.G., 2019. Astronomical time scale for the middle- upper Doushantuo Formation of Ediacaran in South China: implications for the duration of the Shuram/Wonoka negative $\delta^{13}C$ excursion. Palaeogeogr. Palaeoclimatol. Palaeoecol. 532 article #109273: 11 pp. doi:10.1016/j.palaeo.2019.109273.
Sun, Y.B., Clemens, S.C., An, Z.S., Yu, Z.W., 2006. Astronomical timescale and palaeoclimatic implication of stacked 3.6-Myr monsoon records from the Chinese Loess Plateau. Quat. Sci. Rev. 25, 33–48. https://doi.org/10.1016/j.quascirev.2005.07.005.
Tang, P., Huang, B., Wu, R.C., Fan, J.X., Yan, K., Wang, G.X., Liu, J.B., Wang, Y., Zhan, R.B., Rong, J.Y., 2017. On the upper Ordovician Daduhe Formation of the upper Yangtze region. J. Stratigr. 41, 119–133. (in Chinese with English abstract). http://www.cnki.com.cn/Article/CJFDTOTAL-DCXZ201702001.htm.
Thomson, D.J., 1982. Spectrum estimation and harmonic analysis. Proc. IEEE 70 (9), 1055–1096. https://doi.org/10.1109/PROC.1982.12433.
Tong, J.N., Chu, D.L., Liang, L., Shu, W.C., Song, H.J., Song, T., Song, H.Y., Wu, Y.Y., 2019. Triassic integrative stratigraphy and timescale of China. Sci. China Earth Sci. 62, 189–222. https://doi.org/10.1007/s11430-018-9278-0.

Ueno, K., Hayakawa, N., Nakazawa, T., Wang, Y., Wang, X.D., 2013. Pennsylvanian-Early Permian cyclothemic succession on the Yangtze Carbonate Platform, South China. In: Gasiewicz, A., Slowakiewicz, M. (Eds.), Palaeozoic Climate Cycles: Their Evolutionary and Sedimentological Impact. 376. Geological Society, London Special Publications, pp. 235–267. https://doi.org/10.1144/SP376.5.

Wang, X.F., Stouge, S., Chen, X.H., Li, Z.H., Wang, C.S., Finney, C., Zeng, Q.L., Zhou, Z.Q., Chen, H.M., Erdtmann, B.D., 2009. The Global Stratotype Section and Point for the base of the Middle Ordovician Series and the Third Stage (Dapingian). Episodes 32 (2), 96–113. https://doi.org/10.18814/epiiugs/2009/v32i2/003.

Wang, T.T., Ramezani, J., Wang, C.S., Wu, H.C., He, H.Y., Bowring, S.A., 2016. High-precision U-Pb geochronologic constraints on the Late Cretaceous terrestrial cyclostratigraphy and geomagnetic polarity from the Songliao Basin, Northeast China. Earth Planet. Sci. Lett. 446, 37–44. https://doi.org/10.1016/j.epsl.2016.04.007.

Wang, Z.H., Zhen, Y.Y., Ma, H., Zhang, Y.D., 2018. Ordovician conodonts from the Kuniutan to Pagoda Formations at Chenjiahe and Zhenjin of Yichang, Hubei province, China and their stratigraphic significance. Acta Micropalaeotologica Sinica 35 (1), 13–29 (in Chinese with English abstract).

Wang, X.D., Hu, K.Y., Qie, W.K., Sheng, Q.Y., Chen, B., Lin, W., Yao, L., Wang, Q.L., Qi, Y.P., Chen, J.T., Liao, Z.T., Song, J.J., 2019a. Carboniferous integrative stratigraphy and time scale of China. Sci. China Earth Sci. 62, 135–153. https://doi.org/10.1007/s11430-017-9253-7.

Wang, Y.Q., Li, Q., Bai, B., Jin, X., Mao, F.Y., Meng, J., 2019b. Paleogene integrative stratigraphy and timescale of China. Sci. China Earth Sci. 62, 287–309. https://doi.org/10.1007/s11430-018-9305-y.

Wu, H.C., Zhang, S.H., Jiang, G.Q., Huang, Q.H., 2009. The floating astronomical time scale for the terrestrial Late Cretaceous Qingshankou Formation from the Songliao Basin of Northeast China and its stratigraphic and paleoclimate implications. Earth Planet. Sci. Lett. 278, 308–323. https://doi.org/10.1016/j.epsl.2008.12.016.

Wu, H.C., Zhang, S.H., Feng, Q.L., Jiang, G.Q., Li, H.Y., Yang, T.S., 2012. Milankovitch and sub-Milankovitch cycles of the early Triassic Daye Formation, South China and their geochronological and paleoclimatic implications. Gondwana Res. 22, 748–759. https://doi.org/10.1016/j.gr.2011.12.003.

Wu, H.C., Zhang, S.H., Jiang, G.Q., Hinnov, L.A., Yang, T.S., Li, H.Y., Wan, X.Q., Wang, C.S., 2013a. Astrochronology of the Early Turonian–Early Campanian terrestrial succession in the Songliao Basin, northeastern China and its implication for long-period behavior of the Solar System. Palaeogeogr. Palaeoclimatol. Palaeoecol. 385, 55–70. https://doi.org/10.1016/j.palaeo.2012.09.004.

Wu, H.C., Zhang, S.H., Jiang, G.Q., Yang, T.S., Guo, J.H., Li, H.Y., 2013b. Astrochronology for the Early Cretaceous Jehol Biota in northeastern China. Palaeogeogr. Palaeoclimatol. Palaeoecol. 385, 221–228. https://doi.org/10.1016/j.palaeo.2013.05.017.

Wu, H.C., Zhang, S.H., Hinnov, L.A., Jiang, G.Q., Feng, Q.L., Li, H.Y., Yang, T.S., 2013c. Time-calibrated Milankovitch cycles for the late Permian. Nat. Commun. 4https://doi.org/10.1038/ncomms3452. article #2452: 8 pp.

Wu, H.C., Zhang, S.H., Hinnov, L.A., Jiang, G.Q., Yang, T.S., Li, H.Y., Wan, X.Q., Wang, C.S., 2014. Cyclostratigraphy and orbital tuning of the terrestrial upper Santonian-Lower Danian in Songliao Basin, northeastern China. Earth Planet. Sci. Lett. 407, 82–95. https://doi.org/10.1016/j.epsl.2014.09.038.

Wu, Q., Ramezani, J., Zhang, H., Wang, T.T., Yuan, D.X., Mu, L., Zhang, Y.C., Li, X.H., Shen, S.Z., 2017. Calibrating the Guadalupian series (Middle Permian) of South China. Palaeogeogr. Palaeoclimatol. Palaeoecol. 466, 361–372. https://doi.org/10.1016/j.palaeo.2016.11.011.

Wu, H.C., Fang, Q., Wang, X.D., Hinnov, L.A., Qi, Y.P., Shen, S.Z., Yang, T.S., Li, H.Y., Chen, J.T., Zhang, S.H., 2018. An ~34 m.y. astronomical time scale for the uppermost Mississippian through Pennsylvanian of the Carboniferous System of the Paleo-Tethyan realm. Geology 47, 83–86. https://doi.org/10.1130/G45461.1.

Wu, H.C., Hinnov, L.A., Zhang, S.H., Jiang, G.Q., Chu, R., Yang, T.S., Li, H., Xi, D., Wang, C., 2020. Continental geological evidence for two Solar System chaotic events in the Late Cretaceous. Proc. Natl. Acad. Sci. USA (in press).

Xi, D.P., Wan, X.Q., Li, G.B., Li, G., 2019. Cretaceous integrative stratigraphy and timescale of China. Sci. China Earth Sci. 62, 256–286. https://doi.org/10.1007/s11430-017-9262-y.

Xu, K., Chen, H.H., Huang, C.J., Ogg, J.G., Zhu, J.X., Lin, S.Q., Yang, D.Q., Zhao, P., Kong, L.T., 2019. Astronomical time scale of the Paleogene lacustrine paleoclimate record from the Nanxiang Basin, central China. Palaeogeogr. Palaeoclimatol. Palaeoecol. 532https://doi.org/10.1016/j.palaeo.2019.109253. article #109253: 19 pp.

Xu, Y.C., Jiang, R., Deng, Y.Z., Kemp, D.B., Zhu, Z.M., Yang, Z.Y., Huang, C.J., 2020. A robust geochronology of the Yangtze River Delta based on magnetostratigraphy and cyclostratigraphy of sediment core ZKA2. Palaeogeogr. Palaeoclimatol. Palaeoecol. 541 article #109532: 14 pp. doi:10.1016/j.palaeo.2019.109532.

Xue, W.Q., Li, B., Ellwood, B.B., Tomkin, J.H., Wang, Y., Zhu, Z.M., 2015. High-resolution floating point time scale (FPTS) of Permian Capitanian Stage in South China. Chin. J. Geophys. 58 (6), 611–627. http://html.rhhz.net/Geophy_en/html/20150602.htm.

Yao, X., Hinnov, L.A., 2019. Advances in characterizing the cyclostratigraphy of binary chart-mudstone lithologic successions, Permian (Roadian-lower Capitanian), Chaohu, Lower Yangtze, South China. Palaeogeogr. Palaeoclimatol. Palaeoecol. 539, 258–271.

Yuan, D.X., Shen, S.Z., Henderson, C.M., Chen, J., Zhang, H., Zheng, Q.F., Wu, H.C., 2019. Integrative timescale for the Lopingian (Late Permian): A review and update from Shangsi, South China. Earth-Sci. Reviews 188, 190–209. https://doi.org/10.1016/j.earscirev.2018.11.002.

Zachos, J., Pagani, M., Sloan, L., Thomas, E., Billups, K., 2001. Trends, rhythms, and aberrations in global climate 65 Ma to present. Science 292, 686–693. https://doi.org/10.1126/science. 1059412.

Zhang, Y., Li, M.S., Ogg, J.G., Montgomery, P., Huang, C.J., Shi, Z.Q., Enos, P., Lehrmann, D., 2015. Cycle-calibrated magnetostratigraphy of middle Carnian from South China: Implications for Late Triassic time scale and termination of the Yangtze Platform. Palaeogeogr. Palaeoclimatol. Palaeoecol. 146, 135–166. https://doi.org/10.1016/j.palaeo.2015.05.033.

Zhang, Y., Li, L., Ogg, J.G., 2019a. Pliocene-Pleistocene magneto-cyclostratigraphy of IODP Site 1499 and implications for climate-driven sedimentation in the northern South China Sea. Palaeogeogr. Palaeoclimatol. Palaeoecol. 527, 118–132. https://doi.org/10.1016/j.palaeo.2019.04.029.

Zhang, X.S., Over, D.J., Ma, K.Y., Gong, Y.M., 2019b. Upper Devonian conodont zonation, sea-level changes and bio-events in offshore carbonate facies Lali section, South China. Palaeogeogr. Palaeoclimatol. Palaeoecol. 531 (Part A), article #109219 23 pp. doi:10.1016/j.palaeo.2019.05.041.

Zhang, B., Yao, S.P., Wignall, P.B., Hu, W.X., Liu, B., Ren, Y.L., 2019c. New timing and geochemical constraints on the Capitanian (Middle Permian) extinction and environmental changes in deep-water settings: Evidence from the lower Yangtze region of South China. J. Geol. Soc. 176, 588–608. https://doi.org/10.1144/jgs2018-137.

Zhang, Y.D., Zhan, R.B., Zhen, Y.Y., Wang, Z.H., Yuan, W.W., Fang, X., Ma, X., Zhang, J.P., 2019d. Ordovician integrative stratigraphy and timescale of China. Sci. China Earth Sci. 62, 61–88. https://doi.org/10.1007/s11430-017-9279-0.

Zhang, R., Jin, Z.J., Liu, Q.Y., Li, P., Huang, Z.K., Shi, J.Y., Ge, Y.J., Du, K.F., 2019e. Astronomical constraints on deposition of the Middle Triassic Chang 7 lacustrine shales in the Ordos Basin, Central China. Palaeogeogr. Palaeoclimatol. Palaeoecol. 528, 87–98. https://doi.org/10.1016/j.palaeo.2019.04.030.

Zhang, R., Li, L., Nai, W.H., Gu, Y.S., Huang, C.J., Ogg, J.G., Li, Q.H., Lu, C.X., Wang, Z.X., 2019f. Astronomical forcing of terrestrial climate recorded in the Pleistocene of the western Tarim Basin, NW China. Palaeogeogr. Palaeoclimatol. Palaeoecol. 530, 78–89. https://doi.org/10.1016/j.palaeo.2019.05.039.

Zhang, T., Zhang, C.M., Fan, T.L., Zhu, R., Zhang, L., Tao, J.Y., Gao, Z.Q., Li, M.S., 2020. Cyclostratigraphy of Lower Triassic terrestrial successions in the Junggar Basin, northwestern China. Palaeogeogr. Palaeoclimatol. Palaeoecol. 539https://doi.org/10.1016/j.palaeo.2019.109493. article #109493: 14 pp.

Zhao, L.S., Xiong, X.Q., Yang, F.Q., Wang, Z.P., He, W.H., 2005. Conodonts from the Lower Triassic in the Nantuowan Section of Daxiakou, Xingshan County, Hubei Province. Albertiana 33, 113–114.

Zhao, K., Du, X.B., Lu, Y.C., Xiong, S.P., Wang, Y., 2019. Are light-dark coupled laminae in lacustrine shale seasonally controlled? A case study using astronomical tuning from 42.2 to 45.4 Ma in the Dongying Depression, Bohai Bay Basin, eastern China. Palaeogeogr. Palaeoclimatol. Palaeoecol. 528, 35–49. https://doi.org/10.1016/j.palaeo.2019.04.034.

Zhen, Y.Y., Wang, Z.H., Zhang, Y.D., Bergström, S.M., Percival, I.G., Cheng, J.F., 2011. Middle to Late Ordovician (Darriwilian-Sandbian) conodonts from the Dawangou section, Kalpin area of the Tarim Basin, Northwestern China. Rec. Aust. Mus. 63 (3), 203–266. https://doi.org/10.3853/j.0067-1975.63.2011.1586.

Zhong, Y.Y., Wu, H.C., Zhang, Y.D., Zhang, S.H., Yang, T.S., Li, H.Y., Cao, L.W., 2018. Astronomical calibration of the Middle Ordovician of the Yangtze Block. Palaeogeogr. Palaeoclimatol. Palaeoecol. 505, 86–99. https://doi.org/10.1016/j.palaeo.2018.05.030.

Zhong, Y.Y., Chen, D.Y., Fan, J.X., Wu, H.C., Fang, Q., Shi, M.N., 2019a. Cyclostratigraphic calibration of the Upper Ordovician (Sandbian-Katian) Pagoda and Linhsiang formations in the Yichang area, South China. Acta Geologica Sinica (English edition) 93, 177–180. https://doi.org/10.1111/1755-6724.14282. supp.1.

Zhong, Y.Y., Wu, H.C., Fan, J.X., Fang, Q., Shi, M.N., Zhang, S.H., Yang, T.S., Li, H.Y., Cao, L.W., 2019b. Late Ordovician obliquity-forced glacio-eustasy recorded in the Yangtze Block, South China. Palaeogeogr. Palaeoclimatol. Palaeoecol. 540https://doi.org/10.1016/j.palaeo.2019.109520. article #109520: 16 pp.

Zhou, C.M., Yuan, X.L., Xiao, S.H., Chen, Z., Hua, H., 2019. Ediacaran integrative stratigraphy and timescale of China. Sci. China Earth Sci. 62, 7–24. https://doi.org/10.1007/s11430-017-9216-2.

Zhu, R.X., Pan, Y.X., Shi, R.P., Liu, Q.S., Li, D.M., 2007a. Palaeomagnetic and 40Ar/39Ar dating constraints on the age of the Jehol Biota and the duration of deposition of the Sihetun fossil-bearing lake sediments, northeast China. Cretac. Res. 28, 171–176. https://doi.org/10.1016/j.cretres.2006.06.003.

Zhu, M.Y., Zhang, J.M., Yang, A.H., 2007b. Integrated Ediacaran (Sinian) chronostratigraphy of South China. Palaeogeogr. Palaeoclimatol. Palaeoecol. 254 (1), 7–61.

Zhu, R.K., Cui, J.W., Deng, S.H., Luo, Z., Lu, Y.Z., Qiu, Z., 2019a. High-precision dating and geological significance of Chang 7 tuff zircon of the Triassic Yanchang Formation, Ordos Basin in central China. Acta Geologica Sinica-English Edition 93, 1823–1834. https://doi.org/10.1111/1755-6724.14329.

Zhu, M.Y., Yang, A.H., Yuan, J.L., Li, G.X., Zhang, J.M., Zhao, F..C., Ahn, S.Y., Miao, L.Y., 2019b. Cambrian integrative stratigraphy and timescale of China. Sci. China Earth Sci. 62, 25–60. https://doi.org/10.1007/s11430-017-9291-0.